June 2018

Assessing Bald Cypress (Taxodium distichum) Tree Dynamic Change in USF Forest Preserve Area Using Mixture-Tuned Matched Filtering and Multitemporal Satellite Imagery

Yujia Wang
University of South Florida, yujia2@mail.usf.edu

Assessing Bald Cypress (*Taxodium distichum*) Tree Dynamic Change in USF Forest Preserve Area Using Mixture-Tuned Matched Filtering and Multitemporal Satellite Imagery

by

Yujia Wang

A thesis submitted in partial fulfillment
of the requirement for the degree of
Master of Science
School of Geosciences
College of Art and Science
University of South Florida

Co-Major Professor: Ping Wang, Ph.D.
Co-Major Professor: Ruiliang Pu, Ph.D.
Joni Downs, Ph.D.

Date of Approval:
June 26, 2018

Keywords: Remote Sensing, bald cypress tree, Linear Spectral Unmixing, abundance

TABLE OF CONTENTS

LIST OF TABLES

LIST OF FIGURES

ABSTRACT

Wetlands are the most important and valuable ecosystems on Earth. They are called "kidneys of the Earth". Vegetation change detection is necessary to understand the condition of a wetland and to support ecosystem sustainable management and utilization. It has been a great challenge to estimate vegetation (including bald cypress trees) coverage of the wetland because it is difficult to access directly. Satellite remote sensing technology can be one important feasible method to map and monitor changes of wetland forest vegetation and land cover over large areas. Remote sensing mapping techniques have been applied to detect and map vegetation changes in wetlands. To address spectral mixture issues associated with moderate resolution remote sensing images, many spectral mixture methods have been developed and applied to unmix the mixed pixels in order to accurately map endmembers (e.g., different land cover types and different materials within pixels) fractions or abundance. Of them, Mixture Tuned Matched Filtering (MTMF) is an advanced spectral unmixing method that has attracted many researchers to test it for mapping land cover types including mapping tree species with medium or coarse remote sensing image data. MTMF is a partial unmixing method that suppresses background noise and estimates the subpixel abundance of a single target material. In this study, to understand impacts of anthropogenic (e.g., urbanization) and natural forces/climate change on the bald cypress tree dynamic change, the bald cypress trees cover change in University of South Florida Forest Preserve Area was mapped and analysed by using MTMF tool and multitemporal Landsat imagery over 30 years from 1984 to 2015. To evaluate the MTMF's performance, a tradition

spectral unmixing method, Linear Spectral Unmixing (LSU), was also tested. The experimental results indicate that (1) the bald cypress tree cover percentage in the study area has generally increased during the 30 years from 1984 to 2015, but over the time period from 1994 to 2005, the bald cypress tree cover percentage reduced; (2) MTMF tool outperformed the LSU method in mapping the change of the bald cypress trees over the 30 years to demonstrate its powerful capability; and (3) there potentially exists an impact of human activities on the change of the bald cypress trees although a further quantitative analysis is needed in the future research.

CHAPTER ONE:

INTRODUCTION

Wetlands play a vital role in global ecosystem and human life. Therefore, the conservation and sustainable utilization of wetlands resources is important. Precise monitoring of vegetation changes over time is necessary for achieving sustainable development goals in which remote sensing technology can be used to detect and monitor wetlands vegetation changes. Mixture-tuned matched filtering (MTMF) is a remote sensing data analysis method, which only requires that a target spectrum and background spectrum are known. It is a relatively convenient to detect and map single tree species with appropriate remote sensing data.

1.1 Wetlands

Wetlands are an integral part of a global ecosystem as they can improve water quality, protect shorelines, recharge groundwater, store flood water and maintain surface water flow during dry periods, and provide unique habitats for many plants and animals (Guo *et al.*, 2017; Zhao *et al.*, 2010). Wetlands often mean a land that shares a boundary between bodies of water and terrestrial zones. Although wetlands only cover about 6% of the Earth's land surface, they play a vital role in the global ecosystem, and thus the conservation and sustainable use of wetlands and their biodiversity are important (Erwin, 2009; Finlayson *et al.*, 1999). However, despite the importance of wetlands, about 50% of wetlands have been lost since the 1900s (Guo

et al., 2017). According to the research report (see Fish & Wildlife Service, 1999), a total of 14% wetland types in South Florida has been reduced from mid-1950s to mid-1980s. About 6600 km^2 of types was eliminated, which represented about 94 percent of the total wetland loss in the State. The primary cause of wetland loss was the drainage for agriculture, accounting for 79 percent of the total conversion. In addition to habitat loss and fragmentation, wetland habitat quality is also threatened.

Changes in forest cover affect the delivery of important ecosystem services, including biodiversity richness, climate regulation, carbon storage, and water supplies (Hansen *et al.*, 2013). Because of this, many forested wetlands around the world are protected and monitored by various agencies and the importance of wetlands is recognized by international treaties such as the Ramsar Convention on Wetlands (Töyrä and Pietroniro, 2005). Vegetation is one of the major characteristics of wetlands. Destruction to the forest vegetation has led to deterioration of ecological environment and global environment change, such as soil degradation and water loss, local environment pollution caused by destroy, increasing of Carbon dioxide content in the atmosphere, global climate warming, decreasing of biodiversity, and so on. Decreasing of wetland forest vegetation and resources would not only cause soil degradation and climate change, but also bring about serious influence on the ecological balance over the whole global. Protection and restoring of forest vegetation and resources are of practical and long-standing significance (Qiao *et al.*, 2004). It has been a great challenge to estimate vegetation coverage of wetland because they are difficult to access. Given the importance of wetland vegetation in management of wetlands resources in the world, it is necessary to protect wetlands vegetation by detecting and monitoring the distribution and the change of wetland vegetation, and thus wetland-related studies are of great importance to protect wetlands and relieve climate change.

1.2 Remote sensing technology

The remote and inaccessible nature of many tropical forest regions limits the feasibility of filed surveying and monitoring methods for large areas, and this problem can be solved by remote sensing techniques (Mousazadeh *et al.*, 2015; Sader *et al.*, 2001). Access to remote forest regions by surface roads or rivers is often limited, and aerial photography is either nonexistent, outdated or infeasible to acquire for large regions (White *et al.*, 2010). Initiatives to monitor land-cover and land-use change are increasingly reliant on information derived from remotely sensed data (Daniel and Steven, 2001). Remote sensing has become an attractive alternative to field surveys in forest inventory because of its lower total cost, greater coverage, and more regular data collection cycle (Mumby *et al.*, 1999; Noujidina and Ustin, 2008; Zhang and Qiu, 2012).

However, the classification of different types of wetlands by using remote sensing technology is difficult because of spectral confusion with other land cover classes (Ozesmi and Bauer, 2014). Multi-temporal remote sensing data can be used to improve the classification of wetlands. Classified satellite imagery and maps produced by aerial photography have been compared with a conclusion that both offer different but complementary information. Change detection studies have taken advantage of the repeat coverage and archival data provided by multitemporal satellite remote sensing. Wetland maps with more details can be acquired using multitemporal satellite imagery. Given a variety of spatial resolutions of satellite remote sensing systems, fuzzy classification, subpixel classification, spectral mixture analysis, and mixtures estimation can be used to provide more detailed information on wetlands (Ozesmi and Bauer, 2014). Landsat remote sensing time-serial data have been the most common source of data for

land-cover classification and change detection due to its long-term data availability and low cost (Feng *et al.,* 2017).

Traditional classification methods, also called per-pixel classification methods, such as supervised method Maximum Likelihood Classification (MLC) or unsupervised method Iterative Self-Organizing Data Analysis (ISODATA), typically develop a signature by combining the spectra of all training set pixel for the research feature. Most of classification methods are based on per-pixel information which ignore the impact of mixed pixel. As a result, they assign one and only one class to each pixel without considering the impact of mixed pixels (Lu and Weng, 2007). The presence of mixed pixels has been recognized as a major problem, influencing the effective use of remotely sensed data in per-pixel classifications. Subpixel classification approaches that consider variations within pixels have been developed to overcome the mixed pixel problem. Of the available subpixel classifiers, Spectral Mixture Analysis (SMA) is a well-established and effective technique to address this mixture problem (Somers *et al.,* 2011). SMA assumes that the spectral value of each pixel is a linear or nonlinear combination of defined spectrally pure materials called endmembers. The output of SMA is a set of fraction images, each of which represents the area proportions (fraction) of one of the endmembers within the pixel (Lu and Weng, 2007). SMA compares each potential end-member with a composite background spectra. These SMA techniques completely unmix each image and report the fractions of all materials present in each pixel. Thus, they require that all spectra would be known for all major background materials in the images, which can be challenging to obtain in a complex and heterogeneous environment (Brelsford and Shepherd, 2014). Somers *et al*. (2011) noted the challenges associated with endmember selection in nearly all SMA approaches, and

covered the wide variety of approaches that have been used to estimate subpixel fractions of the relevant end-members in an image.

Spectral unmixing methods are valuable candidates for detection of plant species in a spectrally mixed context, such as, SAM (Spectral Angler Mapper) and LSU (Linear Spectral Unmixing). However, plant species detection using fully supervised spectral unmixing approaches may be hampered by the necessity to collect multiple endmembers. Such spectral unmixing approaches allow all targets a user choose to be mapped. Unlike complete unmixing, Partial unmixing methods, such as Mixture-Tuned Matched Filtering (MTMF) require only that the spectral endmembers of the target species are known, by suppressing mixed backgrounds and enhancing the target-to-background contrast (Boardman, 1998). This method represents an improved alternative to SMA or LSU analysis for cases where the number of similar spectra are large or where it is problematic to collect spectra of all potential endmember components within the scene. It performs a partial unmixing by finding only the pixels where user choose endmember spectrum is statistically distinct from the average background spectrum. Usually simple matched filtering results in a large number of false-positive errors. The MTMF unmixing approach has three primary analytical steps. First, the minimum noise fraction (MNF) transformation is applied to minimize and reduce noise in the images across all spectral bands. Second, the matched filtering (MF) is applied for abundance estimation. Final MF scores are normally distributed and have a mean of zero. The magnitude of the MF score is the projection of the target spectrum onto the original image after both have been transformed into MNF space, so that a perfect match will have a score of one. MF returns a mixture tuned (MT) score as the number of standard deviations from the mixing line which connects the background mean to the target spectrum. MT scores can be interpreted as unmixing infeasibility. High MT scores or

infeasibility values, which mean a large separation from the signature of the target material, are used to identify false positives (Xu *et al.*, 2017). The complete MTMF procedure is implemented in the Environment for Visualizing Images (ENVI, Exelis, 2017), a commercially available image analysis software package. William and Hunt (2002) used MTMF to estimate canopy cover of leafy spurge from hyperspectral AVIRIS data and get classification accuracies of 75-95 % for large leafy spurge infestations. Glenn *et al.* (2005) also applied MTMF to map leafy spurge in riparian and mixed sagebrush communities in Idaho using HyMap imagery, with an overall accuracy of above 84%. Pontius *et al.* (2005) implemented MTMF to delineate eastern hemlock abundance and identify early tree decline using AVIRIS data. Besides, many researchers have demonstrated the advantages of MTMF method over other traditional spectral unmixing approaches for mapping vegetation abundances/fractions (e.g., Barbosa *et al.*, 2016; Noujdina and Ustin, 2008; Williams and Hunt, 2002).

CHAPTER TWO:

RESEARCH OBJECTIVES AND QUESTIONS

The major objective of this study is to develop a method to determine and assess the dynamic change of bald cypress (*Taxodium distichum)* in University of South Florida (USF) Forest Preserve Area from 1984 to 2015 to understand impacts of anthropogenic (e.g., urbanization) and natural forces/climate change on the cypress tree dynamic (cover percentage) change. These results are intending to assist the Hillsborough County and her citizens to have a better understand and manage wetland forest resources. This research aims to test performance of Mixture Tuned Matched Filtering (MTMF) to estimate changes in distribution of bald cypress trees in USF Forest Preserve Area, Tampa, between 1984 and 2015 by utilizing multitemporal Landsat images. This study will also compare the performance of MTMF with a traditional spectral unmixing method to map bald cypress canopy change. Through this thesis research, we are able to identify an effective method for mapping bald cypress trees even when they are partially obscured from remote sensing measurements because of overstored trees. In order to understand the cypress tree dynamic change better, four questions will be addressed in this thesis research, which include:

- Is the MTMF able to map the spatial distribution of bald cypress using miltitemporal Landsat imagery?
- Does the MTMF have a better performance than other image spectral unmixing tools?

- How accurate for the remote sensing mapped result is when compared with the ground truth dataset?
- What potential driving forces, which drive the bald cypress tree change, can be identified?

Although most studies have demonstrated the performance of MTMF over some traditional spectral unmixing approaches, there still were a few cases that showed the poor performance of MTMF when mapping vegetation abundance. For example, per testing the performance of MTMF, Brelsford and Shepherd *(*2014) measured changes in subpixel vegetation by using MTMF, and they found that when MTMF abundance estimations have been compared with field estimates of target abundance, the results show clear positive correlations between the MF score and the field estimate, but the correlation values are low. The low values indicated that MF score might be a poor predictor of true target abundance. The general goal of this research is to further test whether MTMF has a better performance than a traditional method.

CHAPTER THREE:

BACKGROUND

3.1 Bald cypress landscape

Bald cypress (*Taxodium distichum*) tree is a deciduous conifer, and it grows on saturated and seasonally flooded soils in the lowlands of the Southeastern and Gulf Coastal Plains of the United States. Figure 1 presents a bald cypress landscape in a wetland.

Bald cypress trees always occurs in swamps along flowing river (Wang and Lang, 2009). They have a peculiarity of growth called cypress knees (the low tower-shaped things in Figure 1). These are woody projections of the root system project above the ground or water. Their function was once thought to be to provide oxygen to the roots, which develop in the low dissolved oxygen waters typical of a swamp (Taxodium distichum, 2018). A bald cypress tree will feature an average height of 15.2 to 36.6 m and a spread of 7 to 10 m when mature (Cochran, 2016). It will grow an average of 0.3 to 0.6 m per year in most locations. Bald cypress trees provide habitat for many species. Wild turkey, wood ducks, evening grosbeak and squirrels eat the seeds. Branches provide nesting places for bald eagles and osprey. Rotting knees are used as nesting cavities by warblers. Catfish spawn beneath cypress logs. Bald cypress absorb and slow floodwaters, relieving flood damage to life and property (Taxodium distichum, 2018).

The native range of bald cypress swamps contain a variety of wetland ecosystem throughout southeastern United States, extend from Florida along the eastern coast of the

Atlantic ocean to Delware, and along the Gulf Coast into Louisiana and Texas, and also inland up the Mississippi River (Middleton and Mckee, 2004). The largest remaining old-growth stands are at Corkscrew Swamp Sanctuary, near Naples, Florida and in the Three Sisters tract along eastern North Carolina's Black River. In the northern and more inland part of its range from Delaware and Maryland to Virginia, it is found in groups growing in swamps and is accompanied by other hardwoods (Bald Cypress, 2018). Although bald cypress grows best in warm climates, the natural northern limit of bald cypress tree is not due to the low temperature, but to specific reproductive requirements, and regeneration is limited by freeze damage to seedlings in further north area. Larger trees are able to stand much lower temperatures and lower humidity (Taxodium distichum, 2018).

The single feature that all bald cypress trees share is their habitats with standing water for at least part time of the year. Their seedlings can only germinate on the dry land, so a fluctuating water level is necessary for a cypress system to survive over long periods. Mature bald cypress trees can stand continual flooding. Because cypress occurs in a wide range of wetland systems, it is possible to identify the hydrologic conditions by the trees that grow in association with the cypress. Bald cypress-hardwood associations are indicative of bottomland riverine forests and sloughs that experience a short hydro period (Mitsch and Ewel, 1979).

3.2 Spectral characteristics of bald cypress

The spectral signature is the reflectance characteristics of a certain cover type as a function of wavelength. Each material has a unique signature, and spectral signature can be used for material classification (Duong *et al.*, 2015). In principle, a land cover type can be identified from its spectral reflectance signature if the sensing system has sufficient spectral resolution to

distinguish its spectrum from those of other materials. This premise provides the basis for multispectral remote sensing.

Figure 1. A landscape of bald cypress trees in University of South Florida Forest Preserve Area, Florida, USA.

Bald cypress tree has a spectral reflectance curve (Figure 2) similar to those of general plants/trees spectra. In the visual part of spectrum, from 400 to 700 nm, the reflectance is low, the reflectance increase rapidly in the infrared in the range 700 to 1300 nm, the gradually decreases to a low level at about 2700 nm because of strong absorption by water (Knipling, 1970). Plant pigments, such as chlorophyll and carotene, and xanthophyll have important effects

upon the absorption and reflectance properties of leaves in the visible wavelengths (Gates *et al*., 1965). The reflectance properties in the near infrared (NIR) wavelengths are influenced by the leaf structure of different species (Slaton *et al.*, 2001). However, these reflectance properties are not sufficient to describe the reflectance of vegetation canopies because a vegetation canopy is composed of a mosaic of leaves, background and shadow (Hurcom *et al*., 1996). Although the canopy reflectance is the main determinant of spectral values of vegetation, the biophysical and biochemical factors can influence plant canopy reflectance and their spectral values (Asner, 1998).

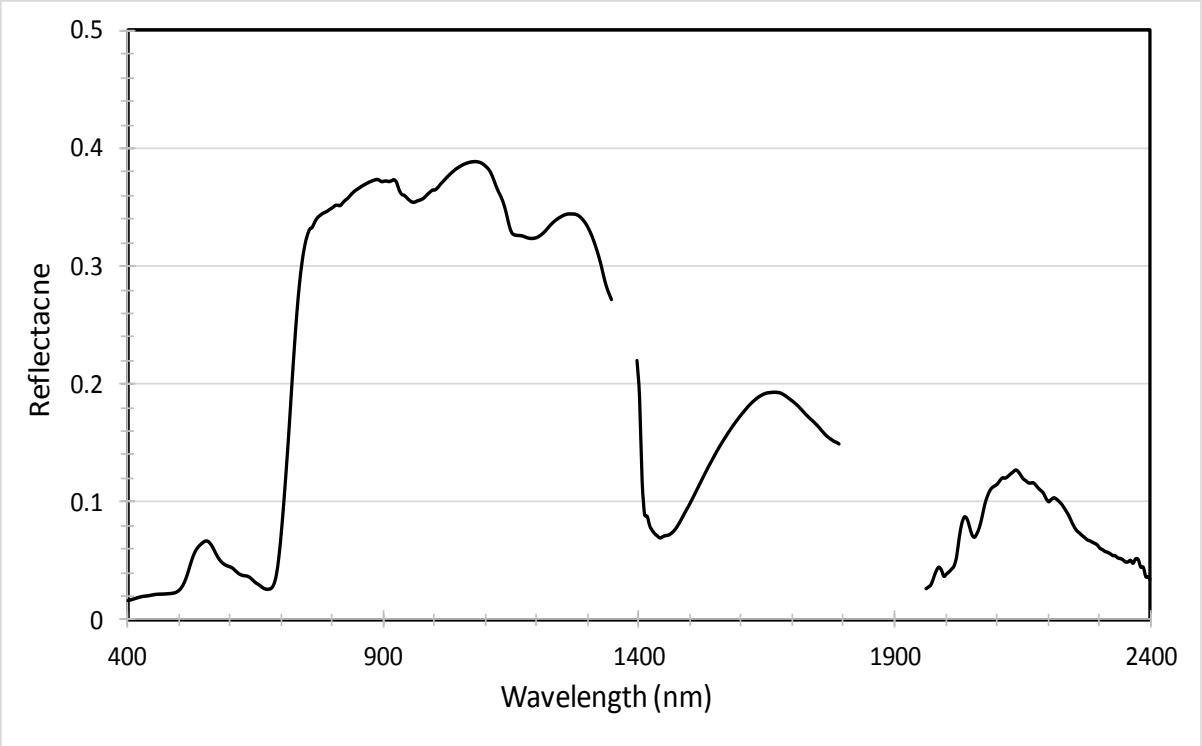

Figure 2. Bald Cypress reflectance of an in situ measurement in a spectral region 400-2400 nm, taken from USF Forest Preserve Area (Provided by Dr. Ruiliang Pu, University of South Florida).

CHAPTER FOUR:

STUDY AREA AND DATA SETS

4.1 Study area

The study area covers the University of South Florida (USF) Forest Preserve Area, a 2 km² tract of region located in Hillsborough County in west central Florida (28° 05'N, 82° 20'W) (Figure 3). More than 50% of the Forest Preserve Area is composed of riverine hardwood swamp forest ("wetland") associated with the Hillsborough River (Wilson, 1998). Hillsborough River flows through the area from west to east within the USF Forest Preserve Area. The rest of the USF Forest Preserve Area is composed of sandhills ("uplands"). There are two kinds of uplands: natural and developed uplands. In the southern portion of the preserve area are uplands of well-drained yellow sand deposits of the Lakeland series that support a xerophytic upland community (Henry, 1985). The sandhill is dominated by slash pine *(Pinus elliottii*), turkey oaks *(Quercus laevis)* and sand live oak (*Quercus geminata*), with a sparse saw palmetto (*Serenoa repens*). Sandhill ecosystems support a wide variety of wildlife. Sandhill habitats are considered to be threatened and endangered in the world. More than 400 plant species are present in the area preserved, including 9 signed as endangered in Florida. These include clasping warea and bent golden aster both listed by the State of Florida as endangered (Cox, 1994).

The USF Forest Preserve Area has a subtropical climate consisting of a 5 month hot and wet season that extends from late spring into the fall, a mild and dry season of 7 months that extends from late fall through spring (Obeysekera, 1999). South Florida's latitude and location

on the eastern shore of a large land mass may lead a sub humid or arid climate, but the region is significantly influenced by the moisture from the Gulf of Mexico, Caribbean Sea. Seasonal high temperatures average about 90s °F (around 32 °C) and lows in the mid-70s °F (around 24 °C), accompanied by high humidity and an almost daily chance of thundershowers, especially in the afternoon. The dry season often begins in November and can last through April. The weather is normally sunny, mild, and quite dry. Highs during the season average around 70 °F (21 °C) with mostly sunny skies. June through November is hurricane season in the Atlantic Basin and Caribbean Sea, with the most tropical activity occurring between mid-august to mid-October. Rain caused by tropical systems is an important component of the area's annual precipitation and is vital for replenishing the water supply of communities around the area. Summers include a high frequency of thunderstorms and lightning, tropical storms, and periodic tornadoes and hurricanes. The cool and dry winters are often punctuated with cold and warm fronts preceded by winds and precipitation that bring brief periods of below or above average temperatures, respectively (Climate of Florida, 2018).

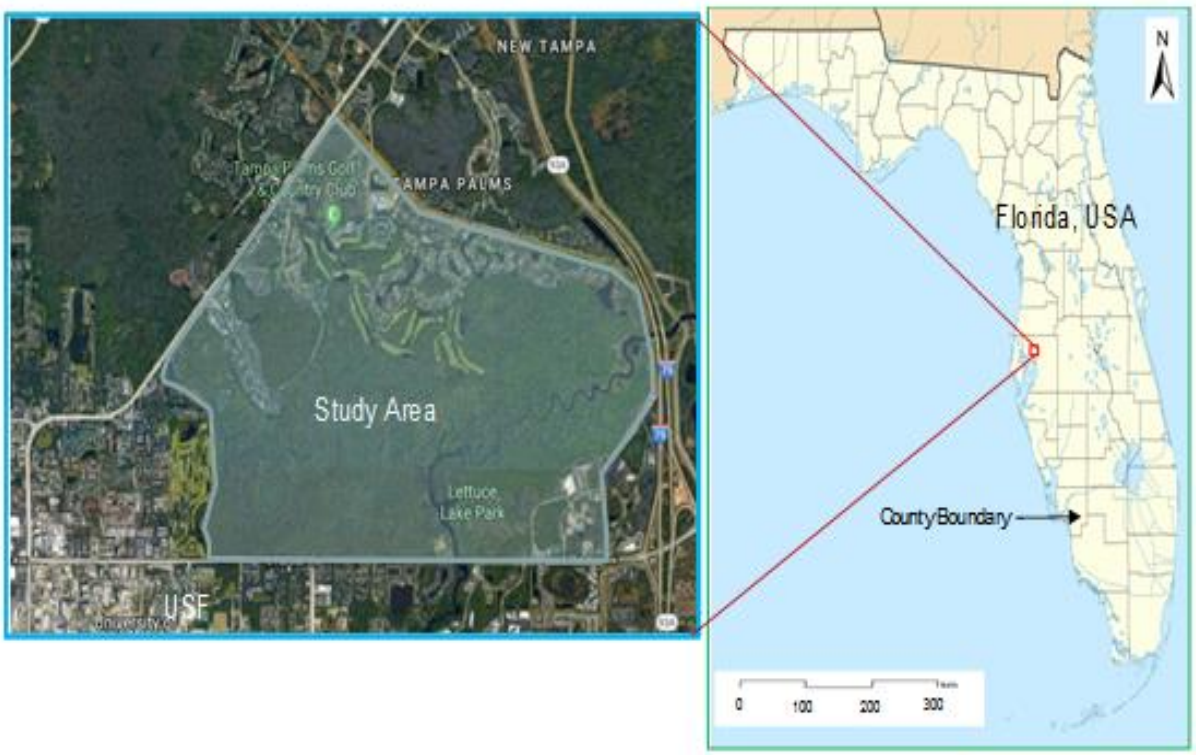

Figure 3. A study map covering the University of South Florida Forest Preserve Area (Provided by Dr. Ruiliang Pu, University of South Florida).

4.2 Data sets

Every five years between 1984 and 2015, the Landsat 5 Thematic Mapper (TM) and Landsat 8 Operational Land Imager (OLI) images were acquired on 1984-10-18, 1994-10-24, 2005-11-23, and 2015-11-03. This is to avoid wet season and minimize the influence of seasonal and weather condition on research area. All processed Landsat images have been geo-rectified within 3 m so that pixels represent the same point in space across all images and the solar irradiance has been normalized across all images. Table 1 summarizes the collection of Landsat images used in this analysis. Figure 4 shows four color composite images using Landsat TM/OLI images NIR/Red/Green bands vs R/G/B.

Table 1. A summary of Landsat images used in this analysis

Path/Row	Acquisition Date	Scene Identifier
17/41	2015-11-03	LC08_L1TP_017041_20151103_20170225_01_T1
17/41	2005-11-23	LT05_L1TP_017041_20051123_20160911_01_T1
17/41	1994-10-24	LT05_L1TP_017041_19941024_20160926_01_T1
17/41	1984-10-18	LT05_L1TP_017041_19841018_20161004_01_T1

Data source: USGS/NASA Landsat Program

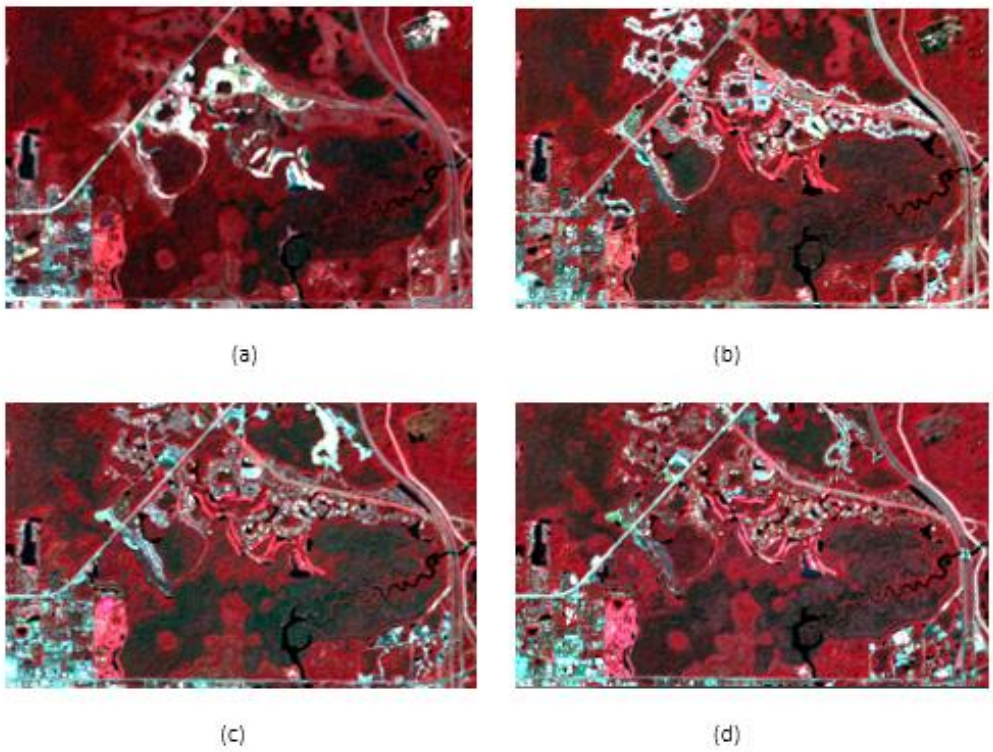

Figure 4. Original color composite images using Landsat TM/OLI images (NIR/Red/Green bands vs. R/G/B color guns) acquired in 1984 (a), 1994 (b), 2005 (c) and 2015 (d)**.**
Data source: USGS/NASA Landsat Program

Table 2. The summary of spatial and spectral information for Landsat TM and OLI images (Jensen, 2016).

Landsat 4 & 5 Thematic Mapper (TM)			Landsat 8 Operational Land Imager (OLI)		
Band	Spectral Resolution(μm)	Spatial Resolution (m) at Nadir	Band	Spectral Resolution(μm)	Spatial Resolution (m) at Nadir
1 Blue	0.45-0.52	30 × 30	1 Ultra-blue for coastal/aerosol	0.433-0.453	30 × 30
2 Green	0.52-0.60	30 × 30	2 Blue	0.450-0.515	30 × 30
3 Red	0.63-0.69	30 × 30	3 Green	0.525-0.600	30 × 30
4 Near-infrared	0.76-0.90	30 × 30	4 Red	0.630-0.680	30 × 30
5 SWIR	1.55-1.75	30 × 30	5 Near-infrared	0.845-0.885	30 × 30
6 Thermal infrared	10.40-12.5	120 × 120	6 SWIR-1	1.56-1.66	30 × 30
7 SWIR	2.08-2.35	30 × 30	7 SWI-2	2.1-2.3	30 × 30
			8 Panchromatic	0.52-0.90	15 × 15
			9 Cirrus	1.36-1.39	30 × 30

CHAPTER FIVE:

METHODOLOGY

In this study, a quantitative analysis method was used to conduct this thesis research. Figure 5 presents a general work flowchart for this study (see page 20). The major components/tasks presented in the flowchart will include: (1) Collect Landsat images for years 1984, 1994, 2005 and 2015; (2) process images: radiometric/geometric correction/registration; (3) run MTMF tool to map bald cypress tree cover/abundance; (4) determine / assess the dynamic change of cypress trees (cover/abundance); and (5) analyze the possible impacts of anthropogenic and natural factors on the change.

5.1 Data preprocessing

Vegetation extraction from remote sensing imagery is the process of extracting vegetation information by interpreting satellite images based on the interpretation elements such as the image color, texture, tone, pattern and association information, etc. Diverse methods have been developed to do this process. Those methods can be supervised or unsupervised depending on whether or not true ground data are inputted as references. General steps involved in vegetation mapping include image preprocessing and image classification. Image preprocessing deals with all preparatory steps necessary to improve the quality of original images, which then

results in the assignment of each pixel of the scene to one of the vegetation groups defined in a vegetation classification system or a membership matrix of the vegetation groups if fuzzy classification is adopted (Xie *et al.,* 2008). Remote sensing signals are essentially the amount of energy received at the sensor from the target in a given spectral width. However, the signals we get directly the satellite are usually noisy. The noise is usually of two types: internal and external noise. Internal noise is from the sensor and external noise from the atmosphere and the areas adjacent to the target. Therefore, it is necessary for us to conduct image preprocessing. Atmospheric correction of satellite images is a critical image-preprocessing step, where the effects of the atmosphere are removed or markedly minimized. A variety of atmospheric-correction algorithms are available. For geometric correction, there are two ways to correct the various types of geometric distortion present in digital image data. One is to model the nature and magnitude of the sources of distortion and use the model to establish correction formulas. That approach is effective when the types of distortion are well characterized, such as that caused by the Earth rotation. The second method depends on establishing mathematical relationships between the addresses of pixels in an image and the corresponding coordinates of those points on the ground. Those relationships can be used to correct image geometric errors irrespective of the analyst's knowledge of the source and type of distortion.

However for this study, Landsat images for years 1984, 1994, 2005 and 2015, provided by USGS, are already Surface Reflectance Level-2 products, which mean that the radiometric correction and geometric correction have been conducted by USGS. The Second Simulation of the Satellite Signal in the Solar Spectrum (6S) model was used for the radiometric correction by USGS to calibrate the Level-1 data to the Level 2 data. Clouds as well as cloud shadows were masked by using Fmask Algorithm (Zhu and Curtis, 2012).

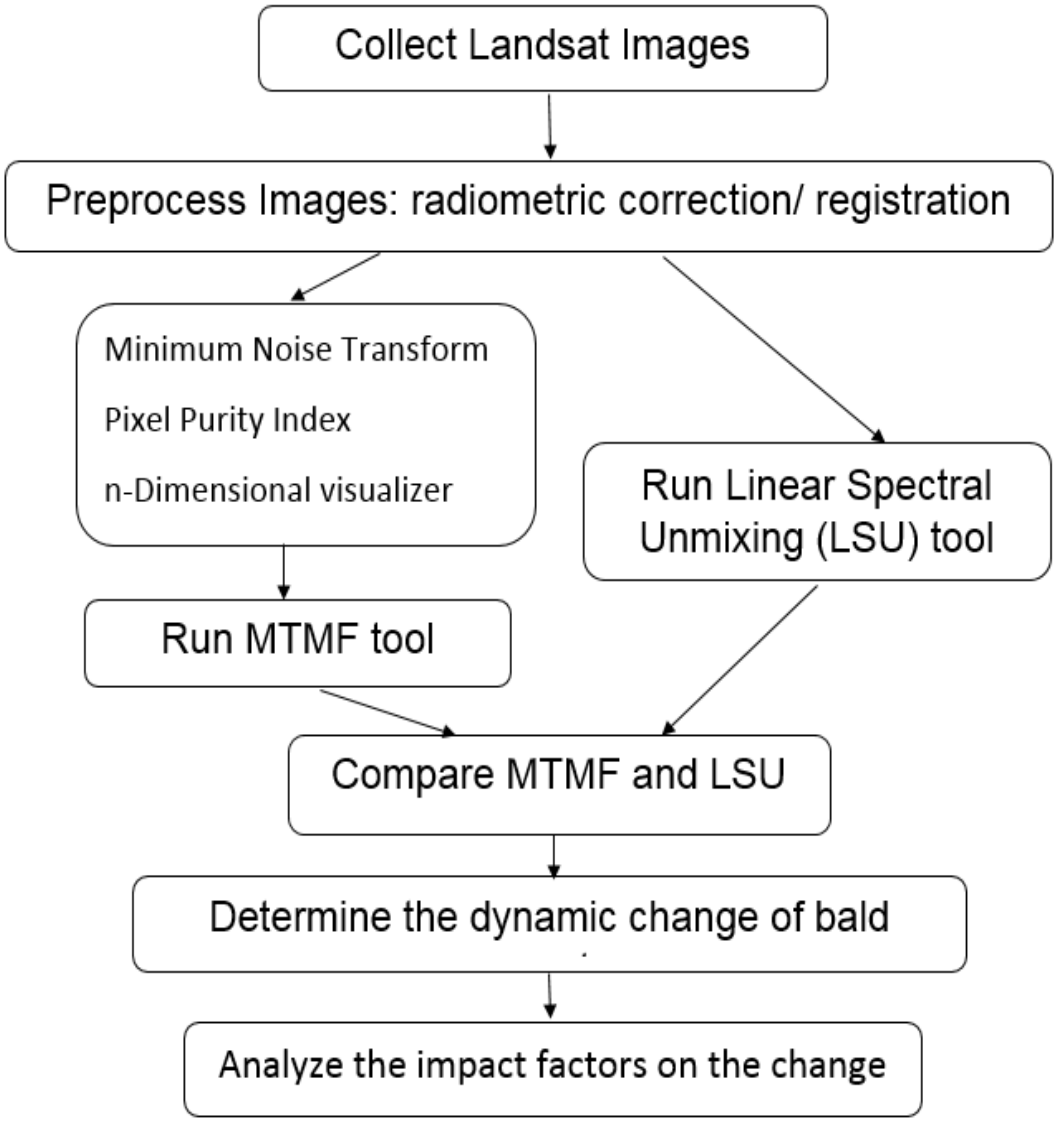

Figure 5. A general work flowchart for this thesis research.

In this study, Landsat image preprocessing also includes the creation of a mask of pixels that were of no interest. Thus, the last step of the image preprocessing in this part was removing any non-interest area around the region of interest (the study area) before conducting further analysis. Figure 6 (b) exactly shows the study area after masking out no interesting areas.

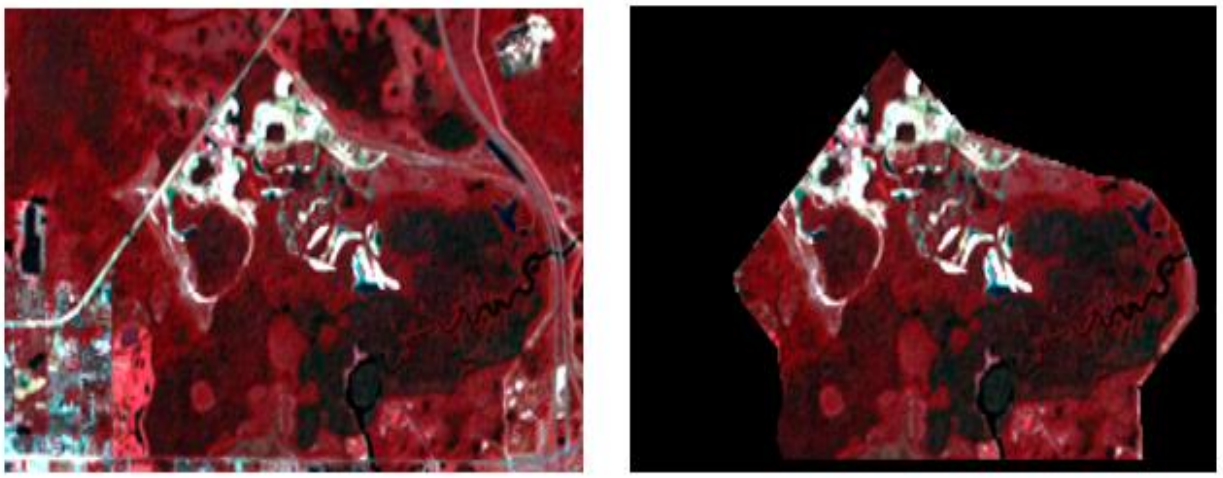

(a) (b)

Figure 6. Masking of the interesting area (i.e., the study area) from a sub-image area. (a) Whole area includes surrounding areas of the study area; and (b) a masked study area only.

5.2 MTMF tool

The analytical process of extracting bald cypress trees fractions in the study area is described as follows.

1) Determine the inner dimensions of image data using the MNF rotation method, and isolate the noises from the data.
2) Calculate the pixel purity index (PPI) to obtain most spectrally pure pixels of bald cypress trees.
3) Input these spectrally pure pixels in the n-D Visualizer to extract endmember spectra.
4) Extract bald cypress abundance of using the MTMF spectral unmixing method.
5) Apply density-slicing method to obtain bald cypress trees fractions.

5.2.1 Minimum Noise Fraction Transformation (MNF)

MNF transform is used to determine the dimensionality of image data and isolate the noises from the data to meet the computing requirements in the subsequent processing. The function of MNF transform in the ENVI software was adopted.

The function of MNF transform is composed of two principal component analysis (PCA) rotations (Qu *et al.,* 2014). The first rotation uses the estimation of noise covariance matrix to reduce and normalize the noise in the data, and generates a band sequence in which the noises have been whitened and their variance is 1, and there is no correlation among bands. The second rotation performs PCA on the band sequence gotten from the firs rotation to organize the components according to the signal-to noise ratio, so the data space will be divided into two parts, one associated with large eigenvalues and coherent Eigen images, and the other one associated with near-unity eigenvalues and noise-dominated images. Then, the coherent Eigen image are selected in the subsequent PPI calculation to separate the noises from the image and improve the processing efficiency.

5.2.2 Pixel Purity Index (PPI)

After MNF transformation, endmembers should be extracted from images as shown in the flowchart**.** According to the definition, an endmember is an idealized pure signature of a class (Chang and Plaza, 2006). In the above-mentioned method for creating a false-colour composite image, it is necessary to define endmembers. These can be defined by the following two methods: (1) automatic definition of training data and (2) selection of endmembers based on the user's knowledge of the study area (Mehr *et al.*, 2013)

Endmember extraction is one of the basic and crucial steps in image processing. It has received a considerable attention in recent years, with many researchers devoting their effort to develop algorithms for endmember extraction from Landsat image. The Pixel Purity Index (PPI) has been widely used in Landsat image analysis for endmember extraction because of publicity and availability in the Environment for Visualizing Images (ENVI) software.

5.2.3 n-Dimensional visualizer

After performing the pixel purity index process, the next step is to visualize those pixels in n-D Visualizer in order to estimate the number of spectral endmembers and their pure spectral signatures (Chuadhry *et al.,* 2006). The n-D Visualizer constitutes a final step in the ENVI endmember-extraction process. The purest pixels obtained from PPI calculation are loaded in the ENVI n-D Visualizer. The selected bands are rotated in the n-D space. When multiple clusters of pixels or corner clusters appear in the view, one or multiple corner pixels are circled to determine the endmembers (Qu *et al.*, 2014).

5.2.4 MF and MTMF

Matched filtering (MF) is a filtering process of input data matching the target spectrum and eliminates the remaining background spectra (Hassan, 2014). Thus, MF performs a partial unmixing of the spectra in each pixel from the analysis image. It distinguishes the target spectra from the background, but does not perform any further analysis on the content of the background materials. As a result of the partial unmixing, MF requires only a target spectrum, not the spectra for all land cover materials in the image, which is one of the major advantages of the MF approach. The mixture tuning (MT) filter has been developed to address cases where MF

generates false positive results; the combined method is called mixture-tuned matched filtering (MTMF) (Bresford and Shepherd, 2014).

The output of MTMF is a set of rule images given as MF score and infeasibility index for each pixel related to each endmember. The MF score results help evaluate the relative consistency of the spectrum and the abundances of sub-pixels. A value of 1 stand for a very high degree of matching (William and Hunt, 2002). The infeasibility index, which is in noise-sigma units, indicates the feasibility of the MF results to be a target endmember. Pixels that have an MF score above the background value and a low infeasibility index are those considered to have a high probability of being identified correctly (Afshar and Saghafian, 2016). The method finds pixels in which the endmember signal is statistically distinct from the average background pixels (Noujdina and Ustin, 2008).

5.3 Linear Spectr Unmixing (LSU)

LSU method is also adopted to determine abundance of land cover classes based on their spectral characteristics. LSU is applied to each pixel using all endmember extracted from an image. The outputs of LSU are a series of fraction images, one for each endmember (Hosseinjani & Tagestani, 2011). A brighter pixel stands for a higher abundance of an endmember in the pixel.

5.4 Accuracy assessment

Theoretically, in order to assess the performance of MTMF, the agreement between results mapped from MTMF and the ground truth data should be determined. However, in this study, due to lacking ground truth data, the test samples of the five land cover types including

bald cypress trees were directly visually delineated from Landsat TM/OLI color composite images (e.g., TM bands 5, 4, 3 vs. R, G, B) via ENVI Region of Interest (ROI) tool. Recently, a visit to the preserve area could help understanding of pure pixels/patches of the five land cover types on the color composite images. Two accuracy indicators were used to evaluate the results of spectral unmixing mapping results. The first indicator is the overall accuracy, and it is total classification accuracy from MTMF. The second indicator is the kappa coefficient, which illustrates the agreement of the ground-surveyed vegetation coverage with the vegetation fraction inversed from MTMF (Qu *et al.*, 2014). When the kappa value > 0.80, it represents a strong agreement and a better accuracy, while when 0.40-0.80, it is medium and when < 0.40, it is poor. In this study, when a pixel value on a fraction image (e.g., bald cypress tree) is greater than 0.8, the pixel is counted as a pure pixel (i.e., suppose 100% covered by only one land cover type).

CHAPTER SIX:

RESULTS

There are two sets of spectral unmixing results for mapping bald cypress cover/abundance extracted from multi-temporal Landsat TM images acquired in 1984, 1994, 2005 and Landsat OLI image acquired in 2015. The two spectral unmixing mapping results of bald cypress trees include those created with MTMF method and those created with a traditional linear spectral unmixing (LSU) method.

6.1 Bald cypress trees abundance estimated using MTMF

The MNF transform is helpful to isolate noise and choose useful MNF components. Typically, the first MNF band represents most of the total variance. The higher-order bands with decreasing variances are not necessary to represent the majority of the original image. Bands with large eigenvalues (greater than 2) contain data, and bands with small eigenvalues contain noise. The screen captures (Figure 7) are useful to distinguish between useful MNF components and noise components. MNF1 possessed the maximum Eigen value and variance (44%, Table 3) that can be considered to be most similar to the original image. Similarly the lower Eigen values and variance (< 6%) components (MNFs 5 and 6) represent too much noise in the images (Figure 8). For this reason, MNFs 5 and 6 were deleted from this analysis.

The MNF results for the 1984 Landsat image are provided in Figure 8 (a)-(f), which demonstrate that higher-numbered bands contain more noise and significantly reduced image features, whereas the lower-numbered bands offer substantially higher information content. Lower numbered bands also correspond to higher eigenvalues.

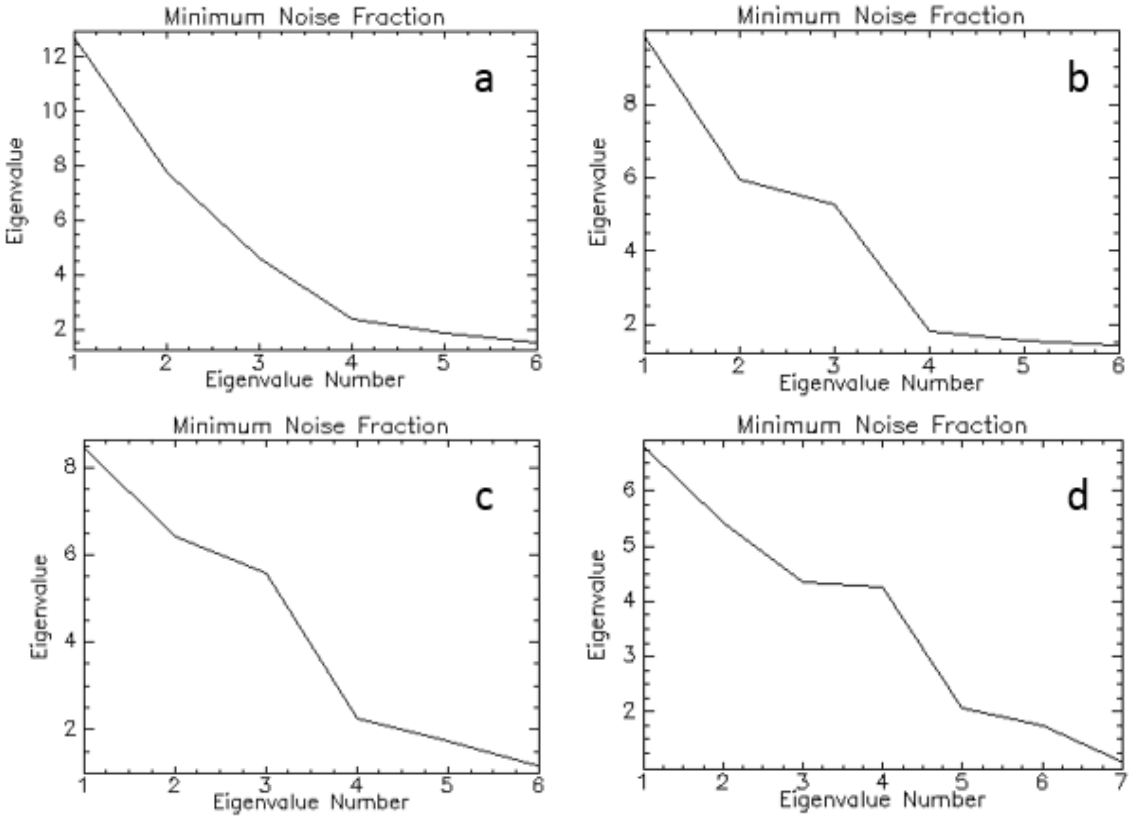

Figure 7. Eigenvalues calculated by the MNF transform analysis.

MNF plot (a) was calculated from the 1984 Landsat image, whereas (b), (c), and (d) represent the MNF transformation results derived from 1994, 2005 and 2015 images, respectively. The first 4 Eigen images were used for further analysis and accounted for most of the useful image information from 1984, 1994, and 2005 Landsat images. The last plot derived from 2015 image shows that the first five bands should be considered.

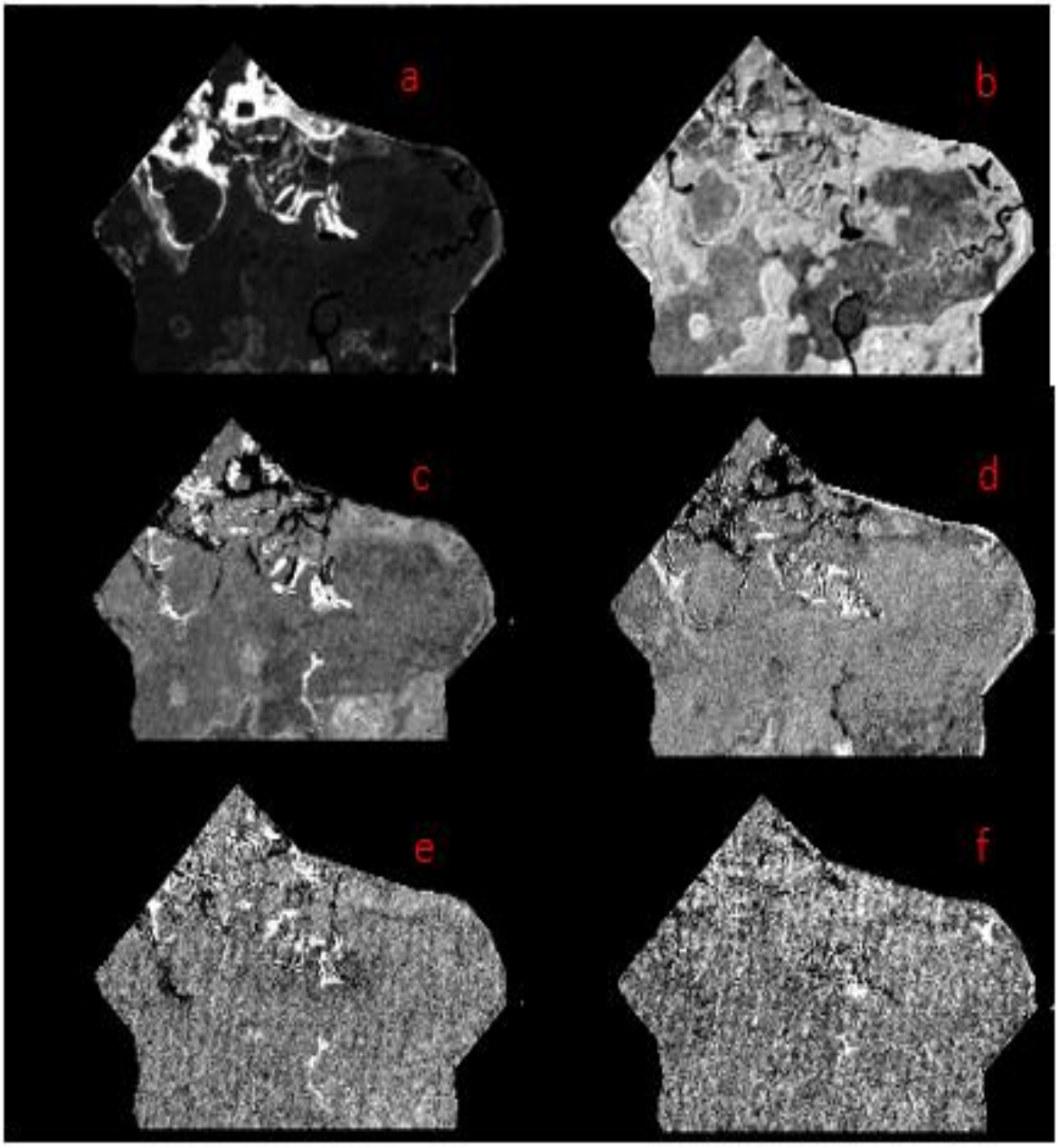

Figure 8. The six MNF feature images derived from 1984 Landsat image. (a)- (f) Images stand for the resultant spectral features (MNFs 1, 2, 3, and 4) and noise (MNFs 5 and 6) components of the MNF transform.

Table 3. The eigenvalues and the associated variance of the MNF components derived from 1984 TM imagery.

Component	Eigen value	Cumulative variance (%)
1	12.68	44.21
2	7.80	66.64
3	4.64	81.52
4	2.39	89.20
5	1.85	95.20
6	1.50	100.00

The PPI was implemented to find endmembers for the image scene in Figure 9 (a), using the same set of randomly generated initial skewers. Figure 9 (b) shows the endmember pixels extracted by the PPI in white. The iterative algorithm, which is the means of finding the most "spectrally pure" or extreme pixels in the multispectral and hyperspectral images, can be used to calculate PPI (Qu *et al.*, 2014). When calculating PPI, the number of iterations is typically large. Therefore, 200, 1000, 3000, and 10 000 iterations were carried out separately. The results of these calculations were approximately same. Among them, the results from 200, 1000, and 3000 iterations are almost same (Figure 10). In consideration of the cost of computing and system load, the result of 200 iterations was chosen for use in the next step.

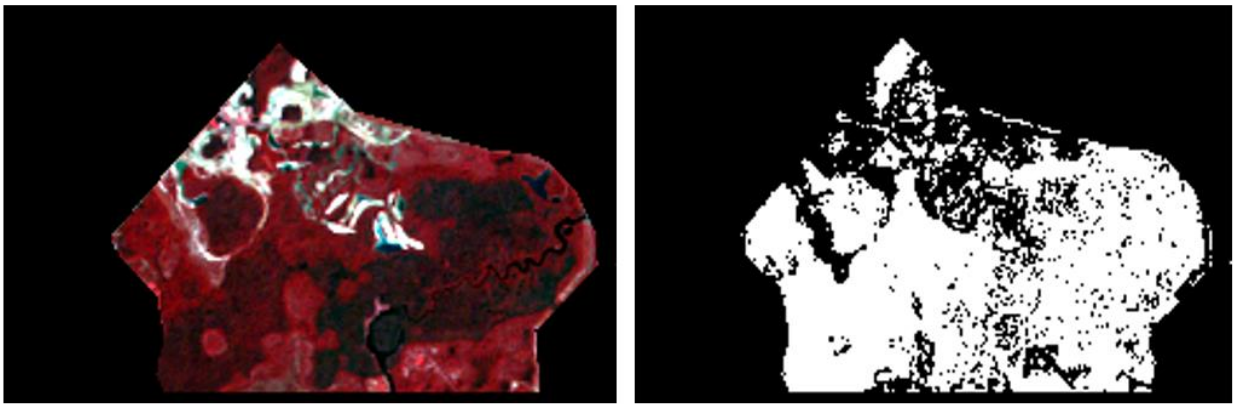

Figure 9. (a) Landsat color composite image acquired in 1984 (RGB vs. TM bands 4, 3, 2), and (b) showing endmember pixels extracted by running a PPI tool.

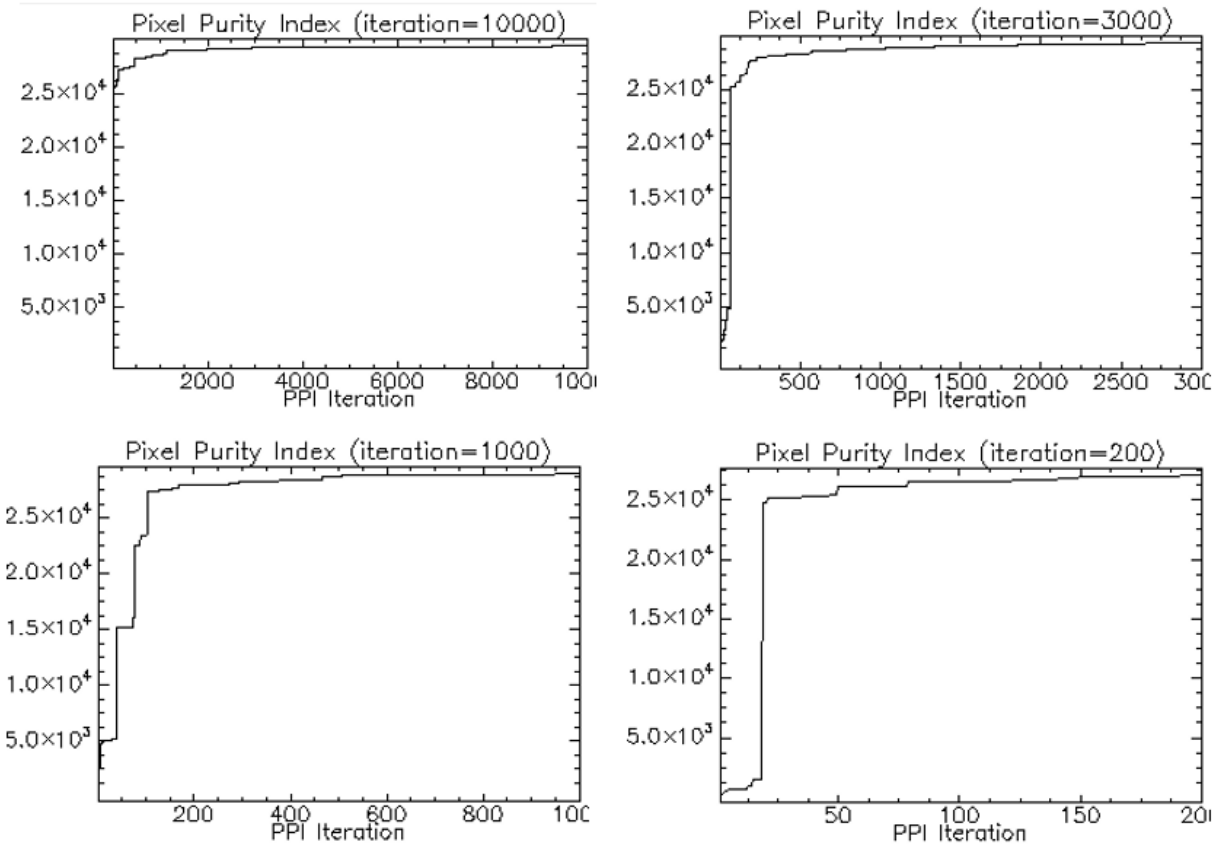

Figure 10. Pixel Purity Index plots derived from Landsat image processing. These four images show the PPI results by iterations10000, 3000, 1000 and 200, respectively.

After running the PPI tool above, an N-Dimensional Visualizer could finally help locate endmember pixels. Displayed on Figures 11 and 12, different endmembers were well separated and could be distinguished in the next analysis. By the simultaneous use of more than two MNF bands, it is possible interactively to view and rotate the endmembers in the n-dimensional spectral space on a screen.

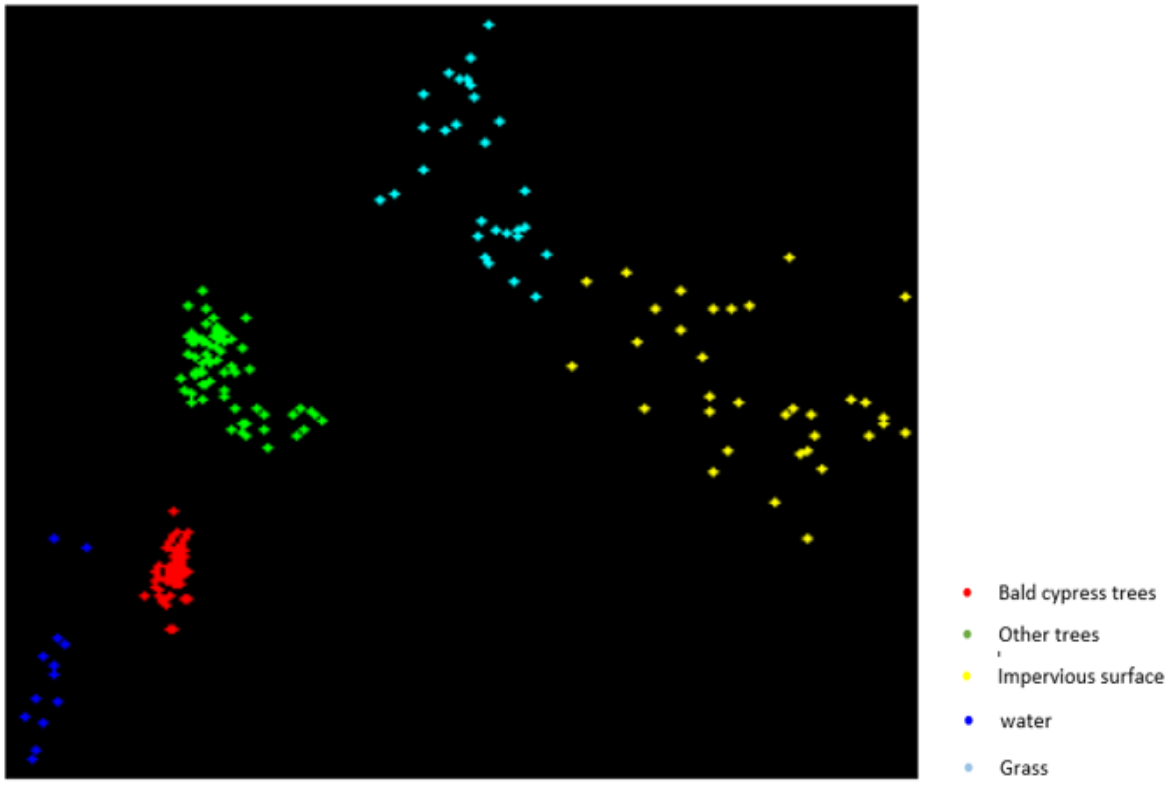

Figure 11. Different endmembers (features) shown in different colors, created with the N-Dimensional Visualizer tool.

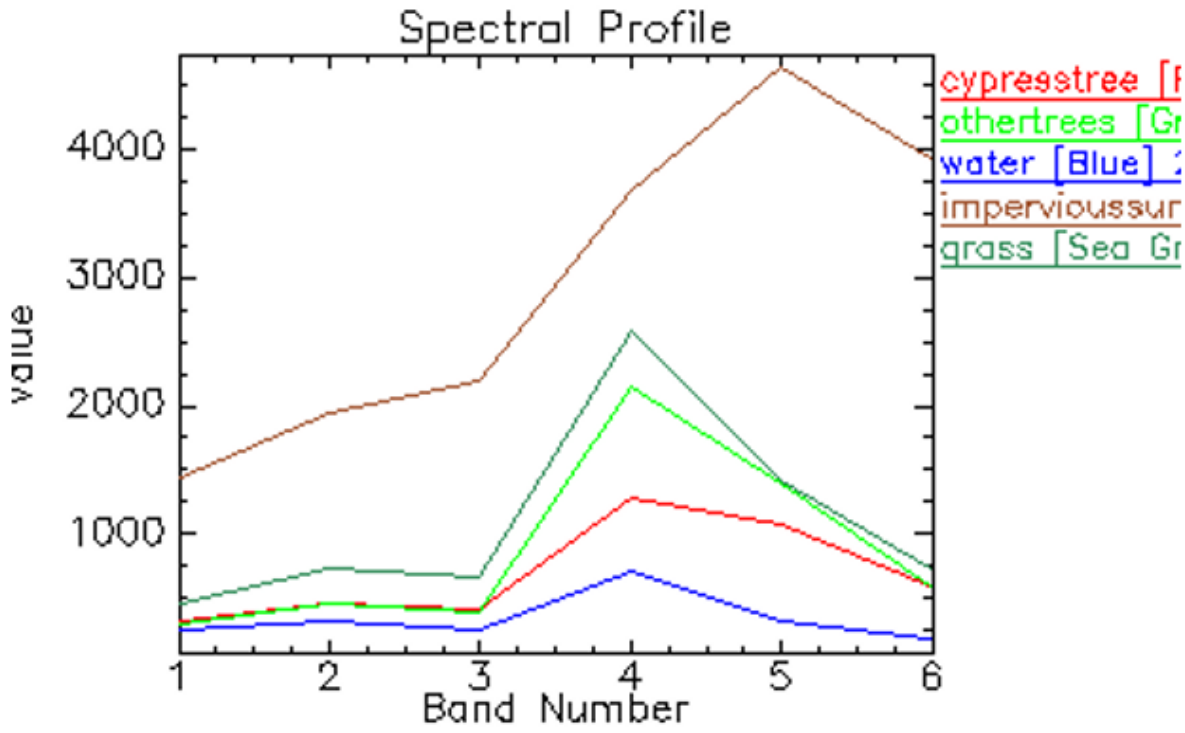

Figure 12. Extracted endmember spectra from the Landsat image (1984). They were used as input to MTMF and LSU spectral unmixing algorithms.

The MTMF outputs consist of a gray-scale two-layer image: the MF score and an infeasibility index (Figure 13). The MF score reflects the relative abundance degree of match between the test (pixel) spectrum and the endmember reference spectrum (e.g., bald cypress). The infeasibility index, which is in noise-sigma units, indicates the infeasibility of the MF results to be a target endmember. Pixels that have an MF score above the background value and a low infeasibility index are those considered to have a high probability of being identified correctly. The pixels have a higher MF score and lower infeasibility index are chosen to shown in the Figure 14 (a) and the outcome is shown in Figure 14 (b), which shows a distribution of pixels with high abundance values of bald cypress trees (in red). The area of the other trees type

exhibited its abundance in the study area with high pixel values in its MF score image (in green in Figure 15a) and had low pixel values in the infeasibility image.

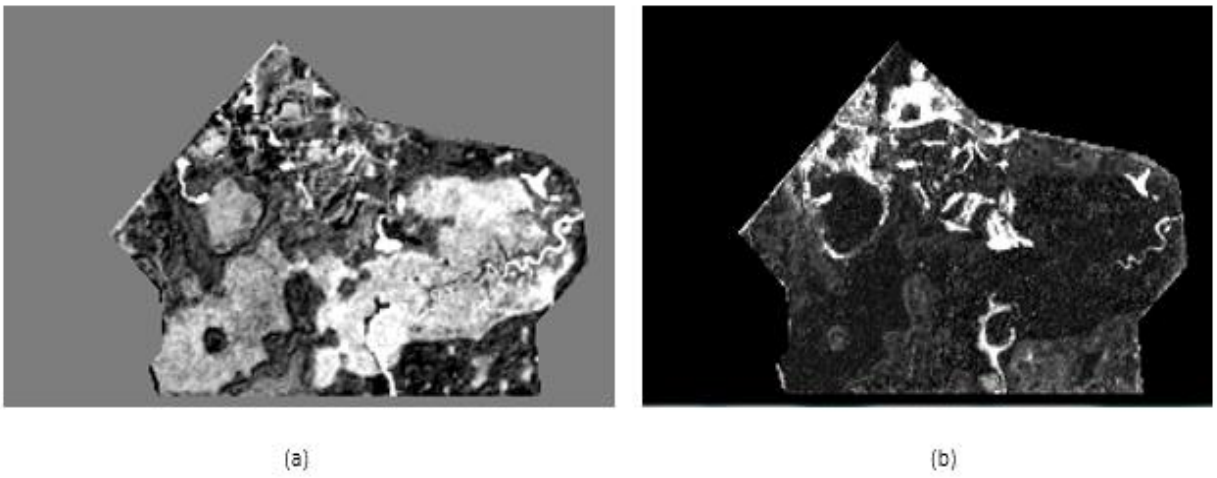

Figure 13. MTMF mapping results: MF score image (a) and infeasibility image (b).

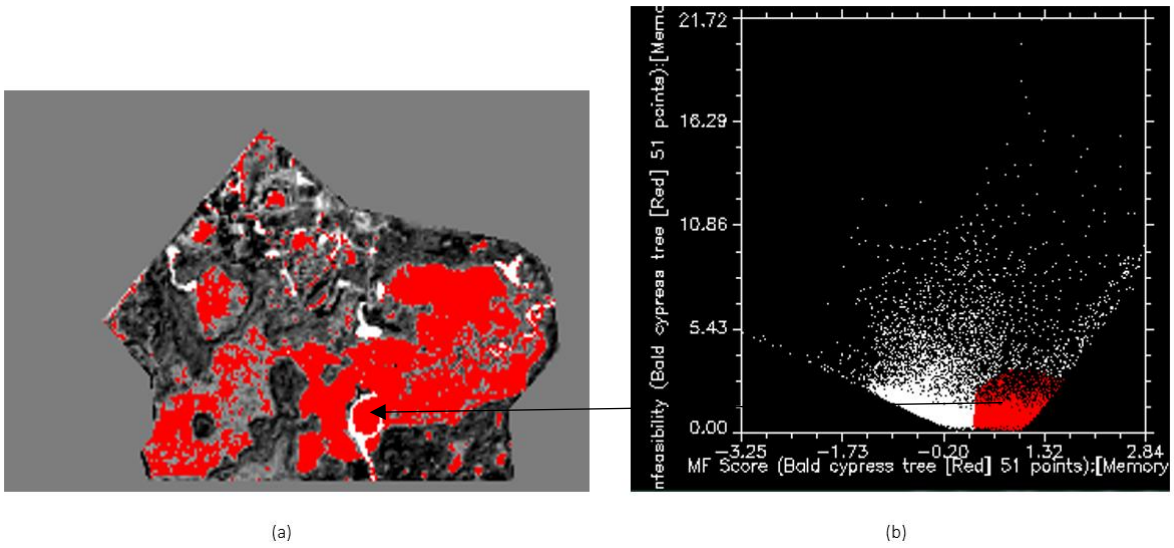

Figure 14. A scatter plot of the matched filter scores versus infeasibility shows that threshold can be used to choose presence target and absence target. The MF demonstrates abundance of bald cypress trees (in red) and the infeasibility value provides a measure of false positives.

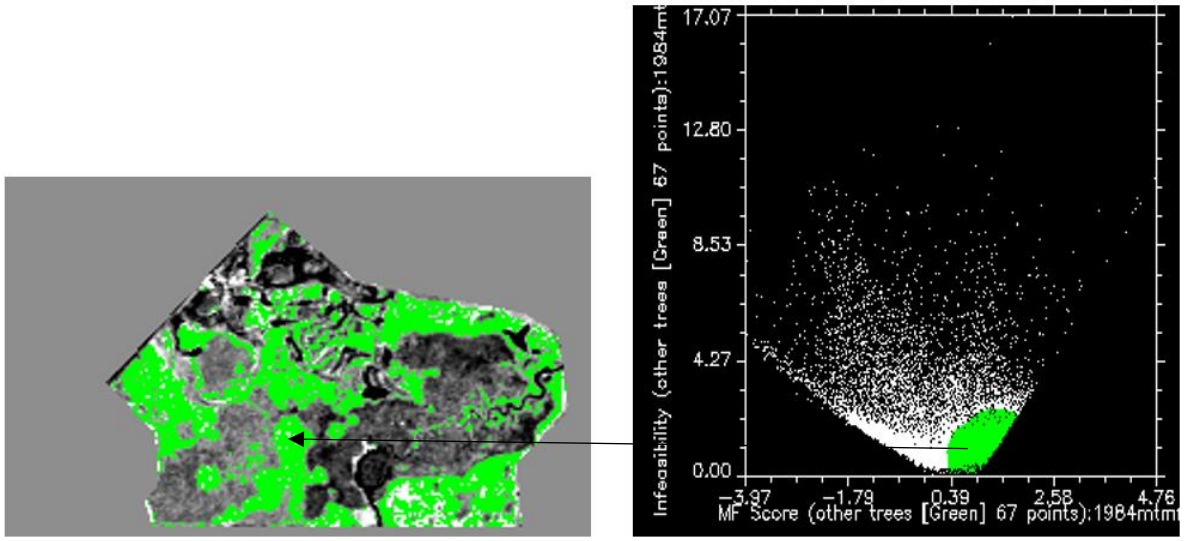

Figure 15. (a) MF score image highlighting the other trees (in green), (b) 2D Scatter-plot of MF score (in green) and MT infeasibility image (in white) for the other trees.

To conduct a dynamic change of bald cypress trees cover/abundance, MTMF derived fractional abundance images from Landsat images were created via an interactive stretching. Abundance estimates for bald cypress trees, other trees, impervious surface, grass and water endmembers are shown as grayscale images (e.g., one in Figure 16). Brighter pixels in the abundance images represent endmembers with higher fractional abundances.

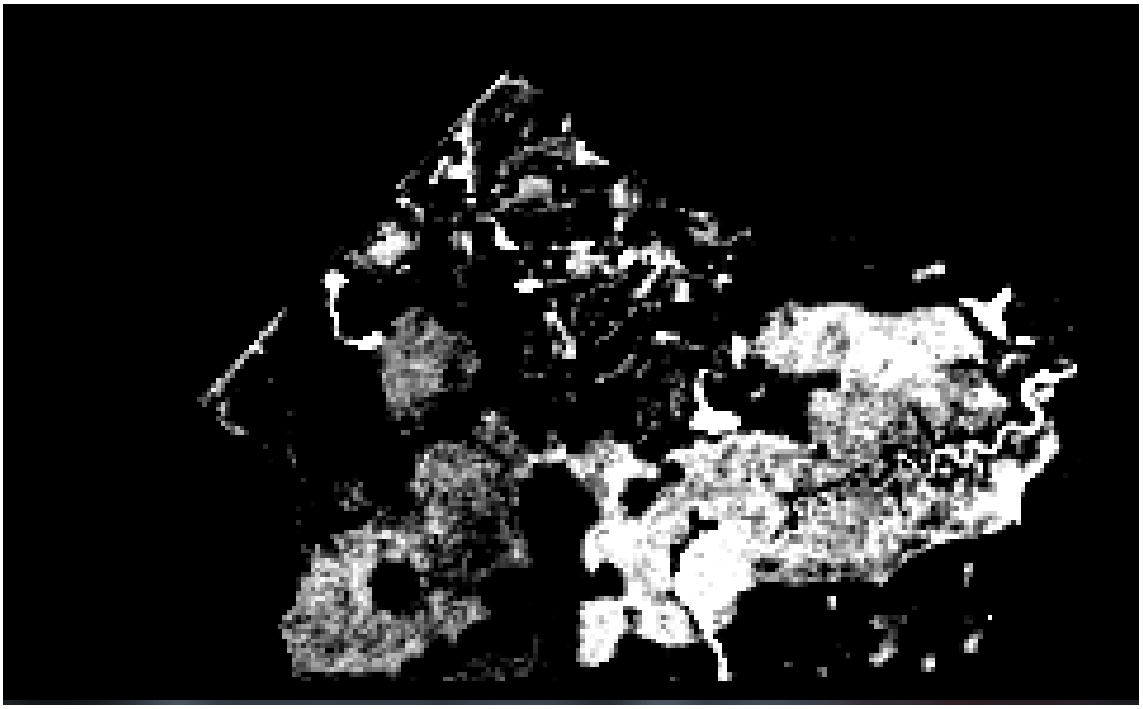

Figure 16. MTMF derived the bald cypress trees fractional abundance image, created from 1984 Landsat TM image. The white degree represents the abundance of an endmember in a pixel.

Finally, MTMF was employed to each Landsat image, which allows false positive to be identified and eliminated from abundance results. The results created from MTMF were in fraction with the sub-pixel abundance values of bald cypress trees and feasibility images that ranging from 0 to 1.5. A pixel with a higher percentage of bald cypress trees in it had a lower infeasibility value, which usually is ≤ 5.00. This is because a low infeasibility value shows a significant MTMF fraction. Figure 17 presents spectral distributions of bald cypress trees in 1984, 1994, 2005, and 2015, and represents the abundances of bald cypress trees in different years, extracted from corresponding Landsat images, respectively. In Figure 17, the black areas stand for no bald cypress tree areas and white areas stand for the areas where bald cypress tree density is extremely high. In Figure 18, a black area has a pixel value -1, which means that bald

cypress trees existed there before but now they are gone. Light color (values close to 1) means that there are more bald cypress trees currently than the before.

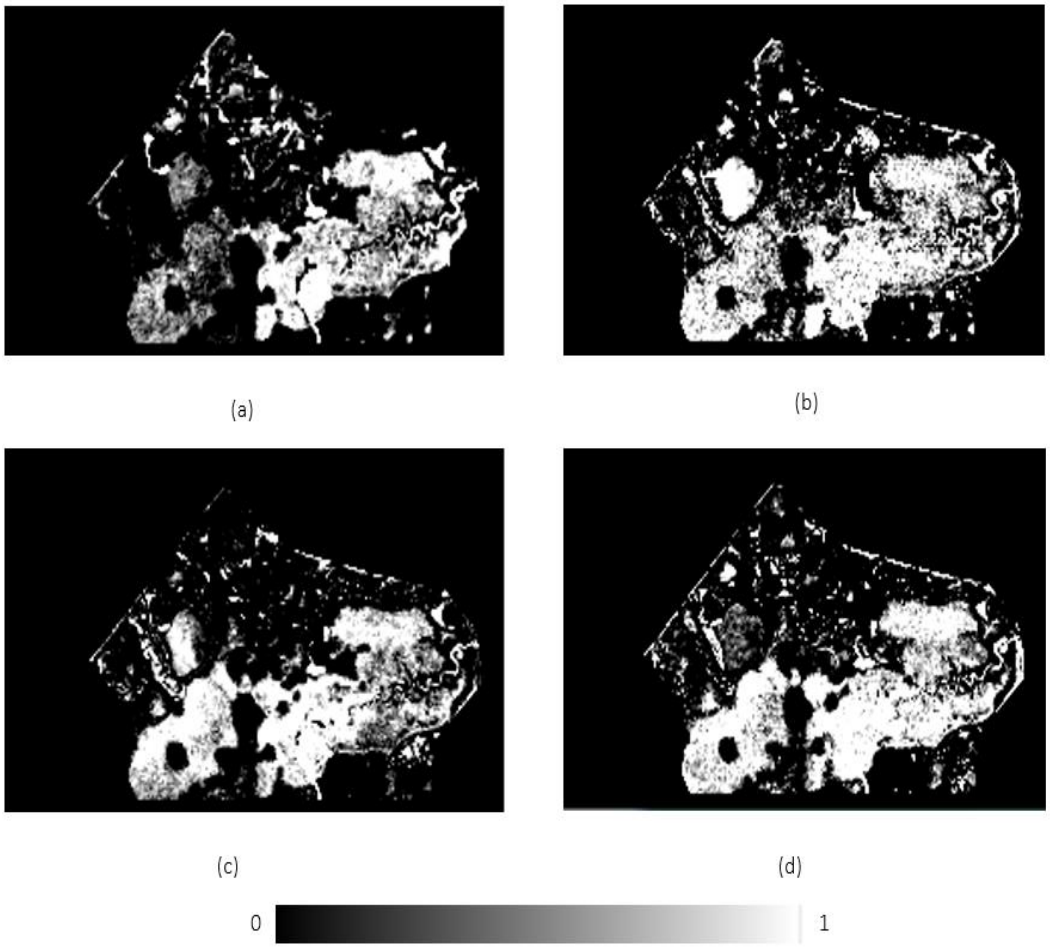

Figure 17. MTMF fraction/abundance images for bald cypress trees. The gray levels for the MTMF fractions: black to white stands for 0 to 1.

From 1984 to 2015 as shown in Figure 18, the bald cypress tree has increased in the research area, especially in the eastern part and western part of the area. Figure 19 clearly indicates that bald cypress trees increased from 26.35% in 1984 to 37.46% in 1994, then decreased to 32.52% in 2005 and then increased again to 37.73% in 2015. Tables 4 and 5

summarize the relative cover percentages of the five land cover types in the four different years and their changes between adjacent two years (i.e., 1984 & 1994, 1994 & 2005, and 2005 & 2015) and 1984 & 2018.

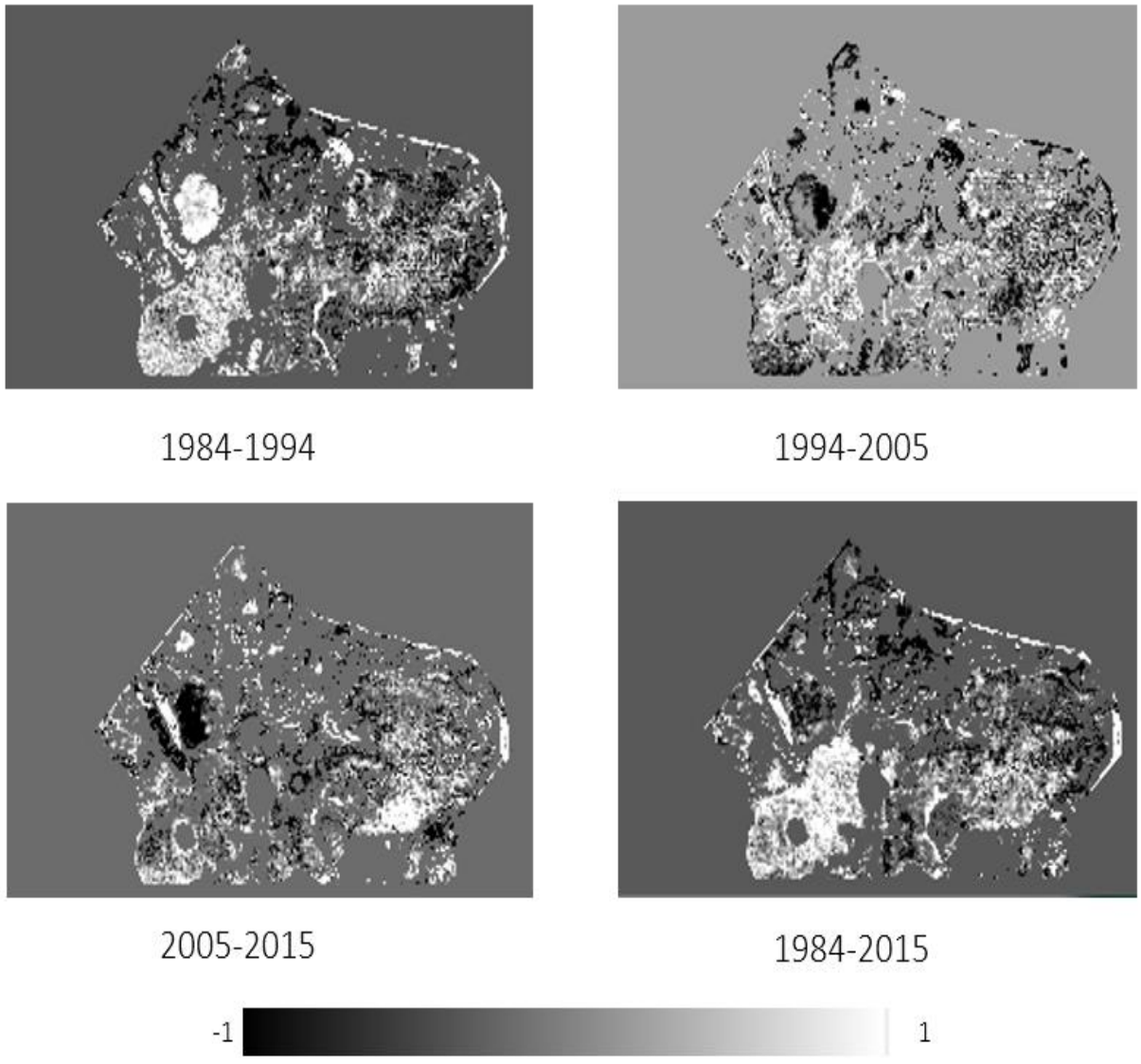

Figure 18. The dynamic change of bald cypress trees in different periods between 1984 and 2015. From gray levels black to white, the values is -1 to 1.

Table 4. Total estimated area of each land cover category (%) in the preserve area.

Land cover category	1984	1994	2005	2015
	Area (%)	Area (%)	Area (%)	Area (%)
Bald cypress tree	26.35	37.46	32.52	37.73
Other trees	35.07	33.04	33.30	30.32
Water	11.30	12.13	11.21	12.43
Impervious surface	13.78	13.82	17.81	15.42
Grass	13.50	3.55	5.16	4.10

Table 5. Land cover changes during the periods of 1984-1994, 1994-2005, 2005-2015 and 1984-2015.

Land cover type	1984-1994	1994-2005	2005-2015	1984-2015
	Area (%)	Area (%)	Area (%)	Area (%)
Bald cypress tree	11.11	-4.94	5.21	11.38
Other trees	-2.07	0.30	-2.98	-4.75
Water	0.83	-0.92	1.22	1.13
Impervious surface	0.03	3.99	-2.39	1.64
Grass	-9.95	1.61	-1.06	-9.40

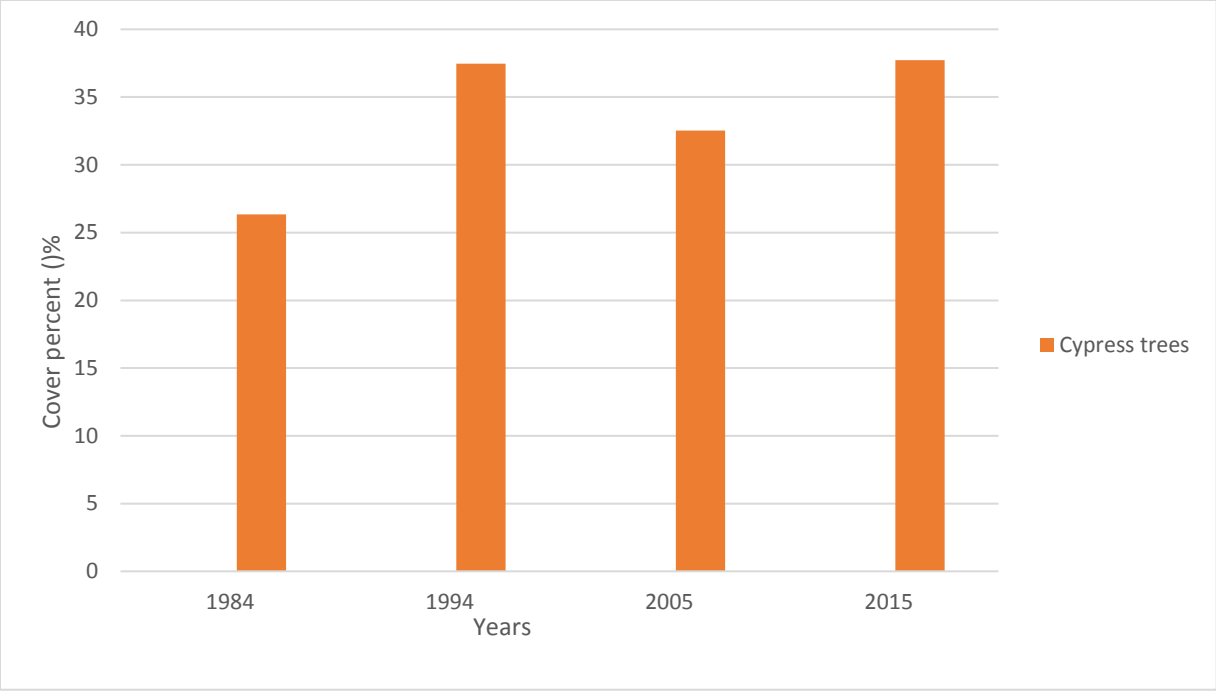

Figure 19. Comparison of cover percentage of Bald cypress trees in different years from 1984 to 2015, created with MTMF from the multitemporal Landsat images.

6.2 Bald cypress trees abundance estimated using LSU

In this thesis research, the traditional LSU approach was also tested for mapping bald cypress tree abundance and its results were used to compare the results created using MTMF. When the same endmember spectra were used for training LSU for different year images as for MTMF, the result in Figure 20 shows bald cypress tree fractions/abundances increased continuously from 34.22% to 45.43% from 1984 to 2005, and then decreased to 40.46 in 2015. The results from LSU share the same trend with the results produced by MTMF, but the percentage of bald cypress trees of each period is higher than that created using the MTMF tool. Compared to those created with the MTMF tool, most uplands with other trees in the results created with the LSU approach were mapped into bald cypress trees. This might be a major error source for LSU derived results compared to those created with the MTMF tool.

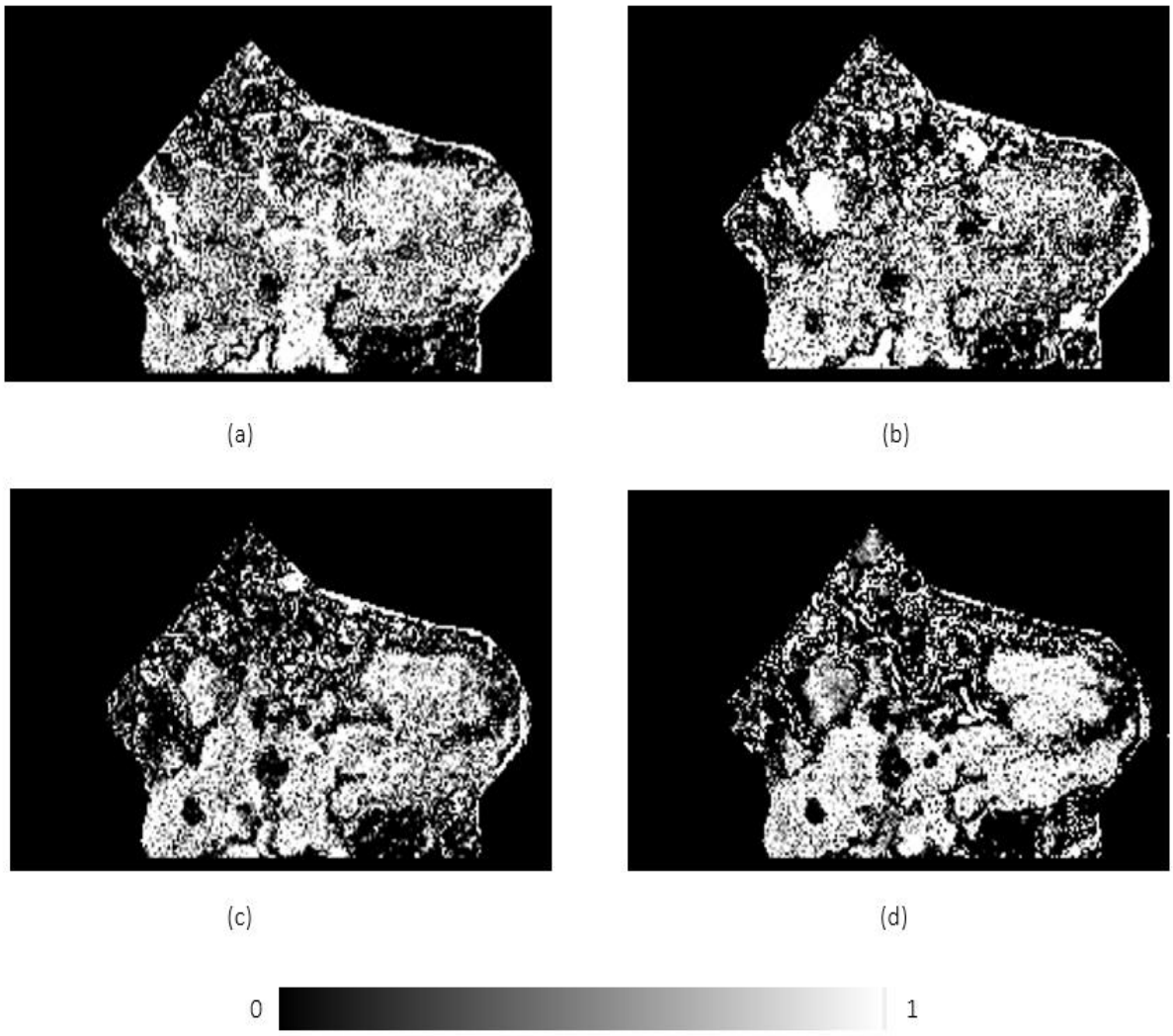

Figure 20. LSU derived fraction images for bald cypress trees. The gray levels for the LSU fractions: black to white stand for 0 to 1.

6.3 The relationship between bald cypress tree and other features

Based on the endmembers (i.e., land cover types in this study) mapping results created with MTMF, the results in Figure 21 indicate that forest (bald cypress trees/ other trees) could account for a large proportion of the study area and water had relatively stable and small proportion, and also impervious surface had a very small proportion of the study area. Overall, water slightly increased continuously from 11.30% to 12.13% from 1984 to 2015; bald cypress

trees increased from 26.35% to 37.46% from 1984 to 1994, then decreased to 32.52% in 2005 and then increased again to 37.73% in 2015; other trees decreased from 35.07% to 33.04% from 1984 to 1994, then increased slightly to 33.30% in 2005, but decreased back to 30.32% in 2015; grass dramatically decreased from 13.50% to 3.55% between 1984 and 1994, then retained a small area; impervious remained steady during the research period. The change of bald cypress trees has a positive correlation trend with water: when the water increased, the bald cypress tree also increased. However, the change of bald cypress trees has an apparent negative correlation trend with other trees, grass and impervious surface.

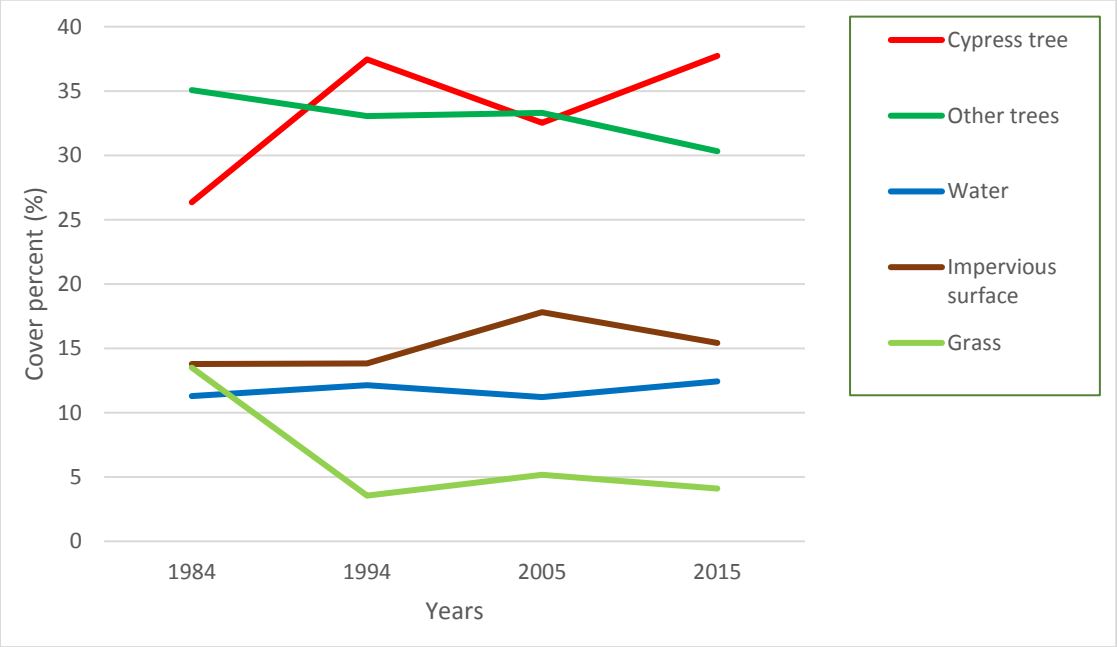

Figure 21. The cover percentages of the five land cover types: bald cypress trees, other trees, grass, impervious surface and water from 1984 to 2015.

6.4 Accuracy assessment

Based upon a total number of 198 test points visually delineated from 2015 OLI image, the accuracy of the five land cover types mapping of the year 1984 was estimated (Tables 6 and 7). Table 6 indicates that MTMF has performed better in distinguishing bald cypress tree, other trees and impervious surface compared to those created with LSU (Table 7). Table 7 presents the mapping results created with LSU. Since the major purpose for this study is mapping bald cypress tree dynamic change over time and testing the performance of the MTMF tool for the purpose, the mapping results listed in Tables 6 and 7 demonstrate that MTMF has showed a better performance compared to LSU and the both Producer's and User's accuracies in mapping the bald cypress trees by MTMF are acceptable in practice.

Table 6. Accuracy assessment for the land cover type mapping results produced by MTMF with 2015 OLI image.

Land cover type	Test result (%)	
	Producer's accuracy (%)	User's accuracy (%)
Bald cypress trees	87.93	100.00
Other trees	56.60	93.75
Water	96.30	100.00
Impervious surface	71.43	100.00
Grass	66.67	100.00

Overall accuracy (OA) = 75.00 %, kappa Coefficient= 0.6989.

Table 7. Accuracy assessment for the land cover type mapping results produced by LSU with 2015 OLI image.

Land cover type	Test result (%)	
	Producer's accuracy (%)	User's accuracy (%)
Bald cypress trees	70.69	85.42
Other trees	59.57	87.50
Water	55.56	75.00
Impervious surface	47.83	84.62
Grass	37.04	76.92

Overall accuracy (OA) = 57.69 %, kappa Coefficient = 0.4931.

CHAPTER SEVEN:

DICUSSION

The results show the bald cypress trees increased from 26.35% to 37.46% from 1984 to 1994, then decreased to 32.52% in 2005 and then increased again to 37.73% in 2015. There are various factors that might cause the fluctuation of bald cypress trees' cover percentage, which has been found in previous research (e.g., Davis, 1997; Othman and Shazali, 2012; Raddi *et al.*, 1994). According to Othman and Shazali (2012), the wetland environments have been interrupted by non-ethical activities such as illegal logging and country development activities that decrease the benefits of the forest contribution. The rapid conversion or degradation of wetland ecosystem is thus of important international concern. Operational systems for monitoring and updating forest maps are thus needed for many applications such as wetland management and habitat monitoring (Desclée *et al.,* 2006). In addition, a preserve area invaded by an exotic species can resulted in the decrease of original species (Cox and Allen, 2011; Makhabu and Marotsi, 2012). Besides, warming temperatures, changing precipitation regimes and diseases are also the causes that generate changes in bald cypress tree species distributions and increases in the duration and severity of pest/pathogen outbreaks. Stone and Finkl (1995) have noticed that bald cypress tree in south Florida is very resistant to hurricane damage. Few trees (4% of all trees sampled) were snapped by Hurricane Andrew happened in 1992 and only 12% of small snapped trees died. Gresham *et al*. (1991) obtained the same result that they found

that cypress foliage was browning, as it does before leaf fall, just before the hurricane struck. The impact of climate on the cypress was also researched by Davis (1997). In the late February 1989, a severe freeze occurred in the north part of the Big Cypress National Swamp, he found that many temperate species had begun new growth but cypress died. According to Manna and Rajchenberg (2004), widespread mortality of cypress occurs throughout its range in Argentina, locally known as 'mal del ciprés'. It was detected about 55 years ago and its extension and importance have increased in the last several decades.

Fire is a key feature of Florida ecosystems, and this is true in the USF forest preserve area. Part of the study area is routinely burned in order to conduct research on ecological succession. A series of plots have been burned at varying intervals since the 1970's, and it happened every year before 1999 (USF Forest Preserve. 2018). This might be the reason why the abundance of Bald cypress tree keep a low level at 1984. In addition, Wang and Lang (2009) found that cypress harvest has risen again because trees on many of the previously harvested old swamps have grown to merchantable size from 1990s. Different from before, landscape mulch has now become one of the main reasons for cypress harvest. This can be used to explain the rapid decrease of bald cypress tree from 1994 to 2005 in the study area. Freezes occurred in January 2001, and most of Florida were hard freezes (National Oceanic and Atmospheric Administration, 2001). Severe freeze may also cause cypress died and it might be the main reason why the bald cypress decreased so fast from 1994 to 2005 in the study area. Bald cypress tree grows well in the areas with lots of water, and the results (Figure 21) shows that the change of bald cypress trees has a positive correlation trend with water, so the change of water area should be another reason why the fluctuation of bald cypress trees area in different periods. Per bald cypress tree cover change over the 30 years (Figure 21, Tables 4 and 5), the reduced

impervious area over time, even small, was associated with surrounding anthropogenic impact on the change of bald cypress cover percentage. Moreover, when the bald cypress tree gradually grown up, the shadow of tree canopy may cover partial impervious surface, which might be a reason why impervious surface decreased from 2005 to 2015. Besides, the difference of acquisition dates of multi-year Landsat images among different years might also slightly cause the change of the bald cypress tree coverage.

CHAPTER EIGHT:

CONCLUSIONS

To map bald cypress tree dynamic change over time, Landsat mage data collected from USGS data center and covering USF Forest Preserve Area in the fall and early winter in 1984, 1994, 2005 and 2015 have been processed and analyzed with two spectral unmixing methods, MTMF and LSU. MNF transform, PPI image generation, and n-D Visualizer have been successfully performed to extract endmember spectra of the five land cover types over the study area. In this study, several preliminary conclusions could be derived from the experimental results:

- The bald cypress tree cover percentage in the research area has generally increased during the 30 years from 1984 to 2015. However, over the time period from 1994 to 2005, the bald cypress tree cover percentage reduced.
- The bald cypress trees has increased in the research area, especially in the eastern part and western part of the area.
- The MTMF outperformed LSU and demonstrated its powerful capability in mapping the changes of bald cypress trees over time.
- There potentially exists an impact of human activities on the change of the bald cypress trees although a further quantitative analysis is needed in the future research.

Wetlands vegetation distribution and its dynamic changes are of important information for making better decisions on wetlands planning and management. However, several challenges in timely and accurately mapping and monitoring the changes of wetlands vegetation and other features should be considered, such as, effects of climate change and human activities on the wetlands changes. Therefore, more research needs to be done to examine how wetland plants distribute spatially and change temporally and drive forces to drive the distribution and change as well.

REFERENCES

Afshar, S., Shamsai, A., & Saghafian, B. 2016. Dam sediment tracking using spectrometry and Landsat 8 satellite image, Taleghan Basin, Iran. Environmental Monitoring and Assessment, 188(2).

Asner, G. P. 1998. Biophysical and biochemical sources of variability in canopy reflectance. Remote Sensing of Environment, 64, 234– 253.

Bald Cypress (Taxodium distichum). https://tpwd.texas.gov/huntwild/wild/species/baldcypress/ , accessed on May 12, 2018.

Barbosa, J., Asner, G., Martin, R., Baldeck, C., Hughes, F., & Johnson, T. 2016. Determining Subcanopy Psidium cattleianum Invasion in Hawaiian Forests Using Imaging Spectroscopy. Remote Sensing, 8(1), 33.

Boardman, J. W. 1998. Leveraging the high dimensionality of AVIRIS data for improved Sub-pixel target unmixing and rejection of false positives: mixture tuned matched filtering. Summaries of the seventh JPL Airborne Geoscience Workshop, 97(1). 55 – 56.

Brelsford, C., & Shepherd, D. 2014. Using mixture-tuned match filtering to measure changes in subpixel vegetation area in Las Vegas, Nevada. Journal of Applied Remote Sensing, 8(1), 083660.

Chang, C., & Plaza, A. 2006. A Fast Iterative Algorithm for Implementation of Pixel Purity Index. IEEE Geoscience and Remote Sensing Letters, 3(1), 63-67.

Chaudhry, F., Wu, C., Liu, W., Chang, C., & Plaza, A. 2006. Pixel purity index-based algorithms for endmemberextraction from hyperspectral imagery. Transworld Research Network, 661(2), 30-62.

Climate of Florida. In Wikipedia, the Free Encyclopedia. https://en.wikipedia.org/w/index.php?title=Climate_of_Florida&oldid=839049332, accessed on May 18, 2018.

Cochran, A. L. 2016. What Is the Growth Speed of the Bald Cypress? http://homeguides.sfgate.com/growth-speed-bald-cypress-47384.html, accessed on May 19, 2018

Cox, J. 1994. Closing the gaps in Florida's wildlife habitat conservation system: Recommendations to meet minimum conservation goals for declining wildlife species and rare plant and animal communities. Tallahassee, FL: Office of Environmental Services, FG & FWFC.

Cox, R. D., & Allen, E. B. 2011. The roles of exotic grasses and forbs when restoring native species to highly invaded southern California annual grassland. Plant Ecology, 212(10), 1699-1707.

Daniel J. H and Steven A. S. 2001. Comparison of Change Detection Techniques for Monitoring Tropical Forest Clearing and Vegetation Regrowth in a Time Series. Photogrammetric Engineering & Remote Sensing, 67(9), 1067-1075.

Davis, S. M. 1997. Everglades: the ecosystem and its restoration. Boca Raton, FL: St. Lucie Press.

Desclée, B., Bogaert, P., & Defourny, P. 2006. Forest change detection by statistical object-based method. Remote Sensing of Environment, 102(1-2), 1-11.

Duong, N. D., Anh, L. V., & Thu, H. L. 2015. Interpretation of land cover using spectral modulation pattern- an example with Landsat 8 OLIimage. Vietnam Journal of Earth Sciences, 36(4).

Erwin, K. L. 2008. Wetlands and global climate change: The role of wetland restoration in a changing world. Wetlands Ecology and Management, 17(1), 71-84.

Exelis, Exelis Visual Information Solutions. 2017. ENVI Image Window Views Help, ENVI5.3

Feng, Y., Lu, D., Moran, E., Dutra, L., Calvi, M., & Oliveira, M. D. 2017. Examining Spatial Distribution and Dynamic Change of Urban Land Covers in the Brazilian Amazon Using Multitemporal Multisensor High Spatial Resolution Satellite Imagery. Remote Sensing, 9(4), 381.

Finlayson, C.M., Davison N.C., Spiers A.G. & Stevenson N.J. 1999. Global wetland inventory-current status and future priorities. Marine and Freshwater Research 50, 717–727.

Fish & Wildlife Service. 1999. Ecological Services | Southeast Region. http://www.fws.gov/verobeach/ListedSpeciesMSRP.html, accessed on May 4, 2018.

Gates, D. M., Keegan, H. J., Schleter, J. C., & Weidner, V. R. 1965. Spectral properties of plants. Applied Optics, 4, 11 – 20.

Glenn, N. F., Mundt, J. T., Weber, K. T., Prather, T. S., Lass, L. W., & Pettingill, J. 2005. Hyperspectral data processing for repeat detection of small infestations of leafy spurge. Remote Sensing of Environment, 95(3), 399-412.

Gresham, C. A., Williams, T. M., & Lipscomb, D. J. 1991. Hurricane Hugo Wind Damage to Southeastern U.S. Coastal Forest Tree Species. Biotropica, 23(4), 420.

Guo, M., Li, J., Sheng, C., Xu, J., & Wu, L. 2017. A Review of Wetland Remote Sensing. Sensors, 17(4), 777.

Hansen, M. C., Potapov, P. V., Moore, R., Hancher, M., Turubanova, S. A., Tyukavina, A., Townshend, J. R. 2013. High-Resolution Global Maps of 21st-Century Forest Cover Change. Science, 342(6160), 850-853.

Hassan, N. 2014. Relative abundance estimations of chengal tree in a tropical rainforest by using modified Canopy Fractional Cover (mCFC). IOP Conference Series: Earth and Environmental Science, 18, 012189.

Henry, R. 1985. Fire and the Florida Sandhill Herpetofaunal Community: With Special Attention to Responses of Cnemidophorus sexlineatus. Herpetologica, 41(3), 333-342.

Hosseinjani, M., & Tangestani, M. H. 2011. Mapping alteration minerals using sub-pixel unmixing of ASTER data in the Sarduiyeh area, SE Kerman, Iran. International Journal of Digital Earth, 4(6), 487-504.

Hurcom, S. J., Harrison, A. R., & Taberner, M. 1996. Assessment of biophysical vegetation properties through spectral decomposition techniques. Remote Sensing of Environment, 56, 203– 214.

Jensen, J. R. 2016. Introductory digital image processing: A remote sensing perspective. Glenview, IL: Pearson Education.

Knipling, E. B. 1970. Physical and physiological basis for the reflectance of visible and near-infrared radiation from vegetation. Remote Sensing of Environment, 1(3), 155-159.

Lu, D., & Weng, Q. 2007. A survey of image classification methods and techniques for improving classification performance. International Journal of Remote Sensing, 28(5), 823-870.

Makhabu, S. W., & Marotsi, B. 2012. Changes in Herbaceous Species Composition in the Absence of Disturbance in aCenchrus biflorusRoxb. Invaded Area in Central Kalahari Game Reserve, Botswana. International Journal of Ecology, 2012, 1-6.

Manna, L. L., & Rajchenberg, M. 2004. Soil properties and Austrocedrus chilensis forest decline in Central Patagonia, Argentina. Plant and Soil, 263(1), 29-41.

Mehr, S. G., Ahadnejad, V., Abbaspour, R. A., & Hamzeh, M. 2013. Using the mixture-tuned matched filtering method for lithological mapping with Landsat TM5 images. International Journal of Remote Sensing, 34(24), 8803-8816.

Middleton, B. A., & Mckee, K. L. 2004. Use of a latitudinal gradient in bald cypress (Taxodium distichum) production to examine physiological controls of biotic boundaries and potential responses to environmental change. Global Ecology and Biogeography, 13(3), 247-258.

Mitsch, W. J., & Ewel, K. C. 1979. Comparative Biomass and Growth of Cypress in Florida Wetlands. American Midland Naturalist, 101(2), 417.

Mousazadeh, R., Ghaffarzadeh, H., Nouri, J., Gharagozlou, A., & Farahpour, M. 2015. Land use change detection and impact assessment in Anzali international coastal wetland using multi-temporal satellite images. Environmental Monitoring and Assessment, 187(12).

Mumby, P. J., Green, E. P., Edwards, A. J. Clark, C. D. 1999. The cost-effectiveness of remote sensing for tropical coastal resources assessment and management, Journal of Environmental Management 55: 157–166.

National Oceanic and Atmospheric Administration. A Review of Weather in 2001 https://www.weather.gov/tae/climate_2001review, accessed on May 6, 2018.

Noujdina, N. V., & Ustin, S. L. 2008. Mapping Downy Brome (Bromus tectorum) Using Multidate AVIRIS Data. Weed Science, 56(1), 173-179.

Obeysekera, J., Browder, J., Horning, L., & Harwell, M.A. 1999. The Natural South Florida System I: Climate, Geology, and Hydrology. Urban Ecosystems. 3(3), 223-244.

Othman, M. F., & Shazali, K. 2012. Wireless Sensor Network Applications: A Study in Environment Monitoring System. Procedia Engineering, 41, 1204-1210.

Ozesmi, S. L., & Bauer, M. E. 2002. Wetlands Ecology and Management, 10(5), 381-402.

Pontius, J., Hallett, R., & Martin, M. 2005. Using AVIRIS to assess hemlock abundance and early decline in the Catskills, New York. Remote Sensing of Environment, 97(2), 163-173.

Qiao, Y., Wang, Y., & Tang, J. (2004). Study of remote sensing monitoring of dynamic change of the Loess Plateau forest resources. Advances in Space Research, 33(3), 302-306.

Qu, L., Han, W., Lin, H., Zhu, Y., & Zhang, L. 2014. Estimating Vegetation Fraction Using Hyperspectral Pixel Unmixing Method: A Case Study of a Karst Area in China. IEEE Journal of Selected Topics in Applied Earth Observations and Remote Sensing, 7(11), 4559-4565.

Raddi, P., Moricca, S., & Paoletti, E. 1994. Effects of Acid Rain and Surfactant Pollution on the Foliar Structure of Some Tree Species. Air Pollutants and the Leaf Cuticle, 205-216.

Sader, S. A., Hayes, D. J., Hepinstall, J. A., Coan, M., & Soza, C. 2001. Forest change monitoring of a remote biosphere reserve. International Journal of Remote Sensing, 22(10), 1937-1950.

Slaton, M. R., Hunt, E. R. Jr., & Smith, W. K. 2001. Estimating near infrared leaf reflectance from leaf structural characteristics. American Journal of Botany, 88, 278– 284.

Somers, B., Asner, G. P., Tits, L., & Coppin, P. 2011. Endmember variability in Spectral Mixture Analysis: A review. Remote Sensing of Environment, 115(7), 1603-1616.

Stone, G. W., & Finkl, C. W. 1995. Impacts of Hurricane Andrew on the coastal zones of Florida and Louisiana, 22-26 August 1992. Fort Lauderdale, FL: Coastal Education and Research Foundation.

Taxodium distichum. In Wikipedia, the Free Encyclopedia. https://en.wikipedia.org/w/index.php?title=Taxodium_distichum&oldid=840244770 , accessed on May 19, 2018.

Töyrä, J., & Pietroniro, A. 2005. Towards operational monitoring of a northern wetland using geomatics-based techniques. Remote Sensing of Environment, 97(2), 174-191.

USF Forest Preserve. 2018. http://facilities.cas.usf.edu/forestpreserve/, accessed on June 27, 2018.

Wang, J., & Lang, P. 2009. Detection of Cypress Canopies in the Florida Panhandle Using Subpixel Analysis and GIS. Remote Sensing, 1(4), 1028-1042.

White, R. A., Dietterick, B. C., Mastin, T., & Strohman, R. 2010. Forest Roads Mapped Using LiDAR in Steep Forested Terrain. Remote Sensing, 2(4), 1120-1141.

Williams, A. P., & Hunt, E. 2002. Estimation of leafy spurge cover from hyperspectral imagery Using mixture tuned matched filtering. Remote Sensing of Environment, 82(2-3), 446-456.

Wilson, D. S. 1998. Nest-Site Selection: Microhabitat Variation and Its Effects on the Survival of Turtle Embryos. Ecology, 79(6), 1884.

Xie, Y., Sha, Z., & Yu, M. 2008. Remote sensing imagery in vegetation mapping: A review. Journal of Plant Ecology, 1(1), 9-23.

Xu, Y., Wang, L., Liu, C., & Liu, C. 2017. Identifying Unlawful Constructions in Cultural Relic Sites Based on Subpixel Mapping—a Case Study in Mangshan Tombs, China. AIMS Geosciences, 3(2), 268-283.

Zhang, C., & Qiu, F. 2012. Mapping Individual Tree Species in an Urban Forest Using Airborne Lidar Data and Hyperspectral Imagery. Photogrammetric Engineering & Remote Sensing, 78(10), 1079-1087.

Zhao, H., Cui, B., Zhang, H., Fan, X., Zhang, Z., & Lei, X. 2010. A landscape approach for wetland change detection (1979-2009) in the Pearl River Estuary. Procedia Environmental Sciences, 2, 1265-1278.

Zhu, Z., & Woodcock, C. E. 2012. Object-based cloud and cloud shadow detection in Landsat imagery. Remote Sensing of Environment, 118, 83-94.